Quaternary International xxx (xxxx) xxx–xxx

Contents lists available at ScienceDirect

Quaternary International

journal homepage: www.elsevier.com/locate/quaint

Using paleoseismology and tephrochronology to reconstruct fault rupturing and hydrothermal activity since c. 40 ka in Taupo Rift, New Zealand

Remedy C. Loame[a], Pilar Villamor[b], David J. Lowe[a,*], Sarah D. Milicich[b], Adrian Pittari[a], Shaun L.L. Barker[c], Andrew Rae[d], Martha G. Gómez-Vasconcelos[e], Manuel Martinez-Martos[f], William F. Ries[g]

[a] School of Science, University of Waikato, Private Bag 3105, Hamilton, 3240, New Zealand
[b] GNS Science, P.O. Box 30368, Lower Hutt, 5040, New Zealand
[c] School of Natural Sciences, University of Tasmania, Private Bag 79, Hobart, 7001, Australia
[d] GNS Science, Private Bag 2000, Taupo, 3352, New Zealand
[e] Cátedras CONACyT, Instituto de Investigaciones en Ciencias de la Tierra, Universidad Michoacana de San Nicolás de Hidalgo, Morelia, Michoacán, Mexico
[f] Dpto. de Geodinámica, Universidad de Granada, 18071, Granada, Spain
[g] Department of Geography and Regional Research, University of Vienna, A-1010, Vienna, Austria

ARTICLE INFO

Keywords:
Tephrostratigraphy
Active normal fault
Paleoseismology
Geothermal sinter
Volcanism
Late Quaternary

ABSTRACT

The Taupo Volcanic Zone (TVZ) in North Island, New Zealand, is the on-land continuation of the Tonga-Kermadec arc formed in the Quaternary at the obliquely convergent boundary of the Pacific and Australian tectonic plates. The central TVZ is a region of intense silicic volcanism and active rifting with a very high heat flux. Within this zone is a dynamic landscape affected by a dense, active fault network, the Taupo Rift. In this rift, the Ngakuru graben hosts fossil hydrothermal systems in an area parallel to numerous active faults including the east strand of Whirinaki Fault that forms a major structure. Using various geoscientific techniques including mapping, stratigraphy, paleoseismic trenching, and tephrostratigraphy, in conjunction with LiDAR-derived DEMs, we reconstruct and date the fault's rupture history along with hydrothermal activity (including silica-sinter development) since c. 40,000 calendar years ago (40 cal. ka) at a site near Hossack Road called “Meade”. Ages for Kawakawa (c. 25.4 cal. ka), Okareka (c. 21.8 cal. ka), Rotorua (c.15.6 cal. ka), Rotoma (c. 9.4 cal. ka), and Taupo (c. 1.7 cal. ka) tephras enabled us to date five identified fault rupture events using the Meade trench excavation. Slip rates of 2.66 ± 0.77 mm/yr (pre-Kawakawa tephra), 0.28 ± 0.04 mm/yr (between c. 25.4 ka and Taupo) and 0.51 ± 0.19 mm/yr (post-Taupo), and the recurrence interval of ~5500 cal. yr during the last c. 25.4 cal. kyr, all correlate with events of similar ages determined from studies on other trenches on Whirinaki Fault. Intercalated with Tahuna tephra (c. 39.3 cal. ka) and additionally dated at c. 38.9 cal. ka using radiocarbon, the hydrothermal sinter began developing at the Meade site at c. 39 cal. ka and ceased by c. 21.8 cal. ka (marked by Okareka tephra). We examine the causative relationship between fault activity and the development of sinter by comparing the chronology of volcanic eruptions and fault rupturing events with that of sinter formation as recorded in three neighbouring sites, Mangatete, Matthews, and Fitzpatrick. The findings improve understanding of the complex rupture behaviour of faulting and provide evidence for relationships between tectonic and hydrothermal activities, which were additionally influenced by the impacts of climatic change and geomorphic processes on landscape evolution, within the late Quaternary period. The study also exemplifies the unique value of tephrochronology in helping to disentangle complex geological deposits and events in an extremely dynamic part of the Earth's surface (the Taupo Rift).

1. Introduction

World economies are under increasing pressure to become carbon neutral, and hence interest in exploiting geothermal energy as a sustainable renewable resource, both for industrial-domestic heating purposes and for electricity power generation, is generally increasing (e.g., Adams et al., 2015; Nogrady, 2017). Focussing on the natural sustainability and life-cycle of a geothermal system leads to questions

* Corresponding author.
E-mail address: david.lowe@waikato.ac.nz (D.J. Lowe).

https://doi.org/10.1016/j.quaint.2019.02.031
Received 7 November 2018; Received in revised form 20 February 2019; Accepted 20 February 2019

Abbreviations

BP	before present ('present' = AD 1950)
cal	calendar or calibrated
^{14}C	radiocarbon
DEM	digital elevation model
DRE	dense rock equivalent
EPMA	electron probe microanalysis
GIS	geographic information system
HEB	hydrothermal eruption breccia
ka	thousands of (calendar) years BP
KVC	Kapenga Volcanic Centre
kyr	thousands of (calendar) years
LGIT	Last Glacial–Interglacial Transition
LGCP	last glacial coldest period
LiDAR	light detection and ranging
MH	Meade-Hossack single event displacement (refers to events MH1 − 4, younger to older, inferred from Meade trench near Hossack Road)
NZCE	New Zealand Climate Event
OHC	Ohakuri caldera
OVC	Okataina Volcanic Centre
SED	single event displacement
SHCAL	Southern Hemisphere calibration
TVC	Taupo Volcanic Centre
TVZ	Taupo Volcanic Zone

regarding the mechanisms for maintaining geothermal activity, and considerations about the interplay between hydrothermal activity, active faulting, and volcanism. The central Taupo Volcanic Zone (TVZ) of northern New Zealand is a region of intense volcanism and rifting, and is a unique location for these considerations (Chambefort and Bignall, 2016 and references therein). The central TVZ consists of a rifted-arc within continental lithosphere that has formed in response to the oblique subduction of the Pacific Plate beneath North Island on the Australian Plate (Fig. 1; Wilson et al., 1995). It comprises a dynamic and rapidly evolving landscape affected by a dense active fault network, the Taupo Rift − a zone of extensional faulting superimposed on the volcanoes of the TVZ (Villamor and Berryman, 2001; Villamor et al., 2011) − with high extension rates (~7–12 mm/yr; Wallace et al. 2004), time-variable fault slip rates (Nicol et al., 2006), and rapid fault spatial migration/evolution (Villamor et al. 2017). The same region has been impacted by voluminous and very frequent silicic eruptions (Wilson et al., 2009; Leonard et al., 2010; Cole et al., 2014) and associated volcanogenic sedimentary influxes from reworking (e.g., Manville and Wilson, 2004; Manville et al., 2009). Volcanism has also undergone fast spatial evolution (Wilson et al., 2009; Cole et al., 2010; Villamor et al. 2017), indicating a variability of location of heat source (magmatism) with time. The convective heat output from geothermal systems in the central TVZ is exceptionally high at 4200 ± 500 MW (Heise et al., 2007), a heat flux comparable to that in Iceland and Yellowstone, USA (Heise et al., 2010). Several fossil silica sinter sites within the Taupo Rift (Campbell et al., 2001, 2004; Brathwaite, 2003; Kissling et al., 2018), isolated from known areas of geothermal activity, are a consequence of active geological processes. Therefore, the rapidly changing landscape in the central TVZ enhances the possibility of successfully determining the underlying natural sustainability of geothermal activity in the central TVZ and the Taupo Rift. The analysis of fossil sinter areas distributed along the study region offers the opportunity to study the interactive processes between hydrothermal activity (including sinter deposition), active faulting, and volcanism.

In this study, we determine the rupture history of the Whirinaki Fault (Canora-Catalán et al. 2008) within the Taupo Rift at a location where fossil sinter deposits have been displaced by the fault (Holland, 2000). We integrate multiple Quaternary geoscientific techniques to examine possible variability in rates of fault activity to assess whether there is a causative relationship between fault activity and sinter development. Our approach is strengthened by the extraordinarily clear geomorphic expression of active faults in the landscape. We have mapped such faults using high resolution digital elevation models (DEMs) derived from LiDAR data (e.g., Langridge et al., 2014). We use paleoseismic trenching and vibrocoring, together with fault deformation restoration techniques, to assess the number of fault rupture events and fault slip rates (e.g., Berryman et al., 2008). We apply tephrochronology, coupled with radiocarbon dating, to reconstruct and date the fault rupture history and hydrothermal activity since c. 40,000 calendar years ago at a single location (the Meade site). At this site, a number of tephra layers intercalated with sinter deposits have been identified using their stratigraphy, physical character, mafic mineralogy, and glass-shard compositions (e.g., Lowe et al., 2017), thus enabling their correlation with well-dated tephras elsewhere. Such application of tephrochronology is being increasingly recognised as a powerful tool for addressing a wide range of global Quaternary research problems (e.g., Lowe and Alloway, 2015; Lane et al., 2017; Lowe et al., 2017). Very few studies have used tephrochronology to date sinter previously (e.g., Campbell et al., 2004, in New Zealand; Jones et al., 2007, in Iceland), and our study is the first to use the method to constrain ages for both fault rupture and hydrothermal activity (generating sinter formation) at a single site. This integrated approach has helped us to establish potential causative relationships between sinter evolution and the landscape-modifying processes presently active in the central TVZ, including fault rupture, volcanism, and late Quaternary climate change.

Note that all ages in this paper are reported in calendar (calibrated, cal.) years before present (BP), with present taken as AD 1950, unless specified otherwise. In many instances we use the abbreviation 'cal. ka', meaning thousands of calendar years BP, or 'cal. kyr', meaning thousands of calendar years.

1.1. Tectonic setting and paleoseismicity

The Meade trench site at Hossack Road is located within the Ngakuru Graben in the Taupo Rift (Villamor et al., 2011; Fig. 1). The earthquake activity of the Taupo Rift is characterised by small to moderate size earthquake swarms (Hurst et al., 2008), as well as moderate to large earthquakes with a typical main shock-aftershock sequence (e.g., Beanland et al., 1989). Seismicity occurs within a thinned seismogenic crust of 8 km thickness (Bryan et al., 1999; Reyners et al., 2007). The largest historic earthquake had a magnitude of Mw 6.3 (1987 Edgecumbe Earthquake; Beanland et al., 1989), and paleoseismic studies suggest that earthquakes could be as large as Mw 7.0 (Berryman et al., 2008; Canora-Catalán et al. 2008).

The Ngakuru Graben is a 14-km-wide structure formed by active faults which mainly strike 040° (Fig. 1A and E). As the faults approach the Okataina caldera margin to the northeast, the strike bends to 060° (Fig. 1B) (Villamor et al., 2011). These normal faults displace late Quaternary pyroclastic fall and flow deposits and reworked volcanogenic sediments (Nairn, 2002). Several studies have examined fault activity in the Ngakuru Graben to inform earthquake hazard assessment (Berryman et al., 2008; Canora-Catalán et al. 2008) and provide data on fault behaviour (i.e., slip rate, size, and recurrence interval variability; e.g., Nicol et al., 2009). Villamor et al. (2011) examined relationships between the timing of fault rupture within the Ngakuru Graben and eruptive episodes in the Okataina Volcanic Centre (OVC) (see Fig. 13, below), using tephrostratigraphy to constrain fault timing. They concluded that faulting in the Ngakuru Graben is mainly tectonic, whereas dike intrusion (with minor tectonic faulting) dominates the OVC itself.

However, dike intrusion plays a role within the Ngakuru Graben in only some cases, notably at sites < 5 km from volcanic vents. Villamor et al. (2011) also suggested that near-failure faults may have been triggered to rupture by magmatic activity in the area through static stress transfer.

1.2. Whirinaki Fault

The Whirinaki Fault is a north-east-trending, north-west-dipping normal fault on the eastern flank of the Ngakuru Graben (Fig. 1A). Canora-Catalán et al. (2008) described the fault as consisting of two segments, east and west (the latter segment was previously named Puaiti Fault; e.g., Villamor and Berryman, 2001), that merge in depth, which allows for both segments to also rupture together.

Fault single-event displacements vary from 0.2 to 4 m over the past c. 25,400 cal. years, with the overall slip rate increasing from 0.3 mm/yr to 1.3 mm/yr and the rupture recurrence interval decreasing in the last 2000 years (Canora-Catalán et al. 2008). The displacement rates on the Whirinaki Fault, south of the Hossack Road area, have varied over the past 18,000 cal. years, with a range of 0.1–3.6 mm/yr (Canora-Catalán et al. 2008).

In our study area (the Meade site, Figs. 1B and 2A), the Whirinaki Fault displaces thick deposits of the Ohakuri Formation and an overlying sequence of late Quaternary tephras (described below) derived from multiple rhyolitic volcanic eruptions in the central TVZ. The abundance of correlatable tephras of known ages allows for relatively good constraints on fault rupture events because the 'soft' pyroclastic deposits were deformed then covered by further deposits, usually preserving evidence of rupture. At the Meade site, detailed tephra identification was aided by mineralogical and geochemical data because several of the individual tephra layers found in this area were difficult to identify in the field with certainty.

1.3. Paleohydrothermal features

Siliceous sinters are surface features typically associated with geothermal systems that occur as aprons around hot springs and geysers, and form by precipitation of non-crystalline opal-A as silica-

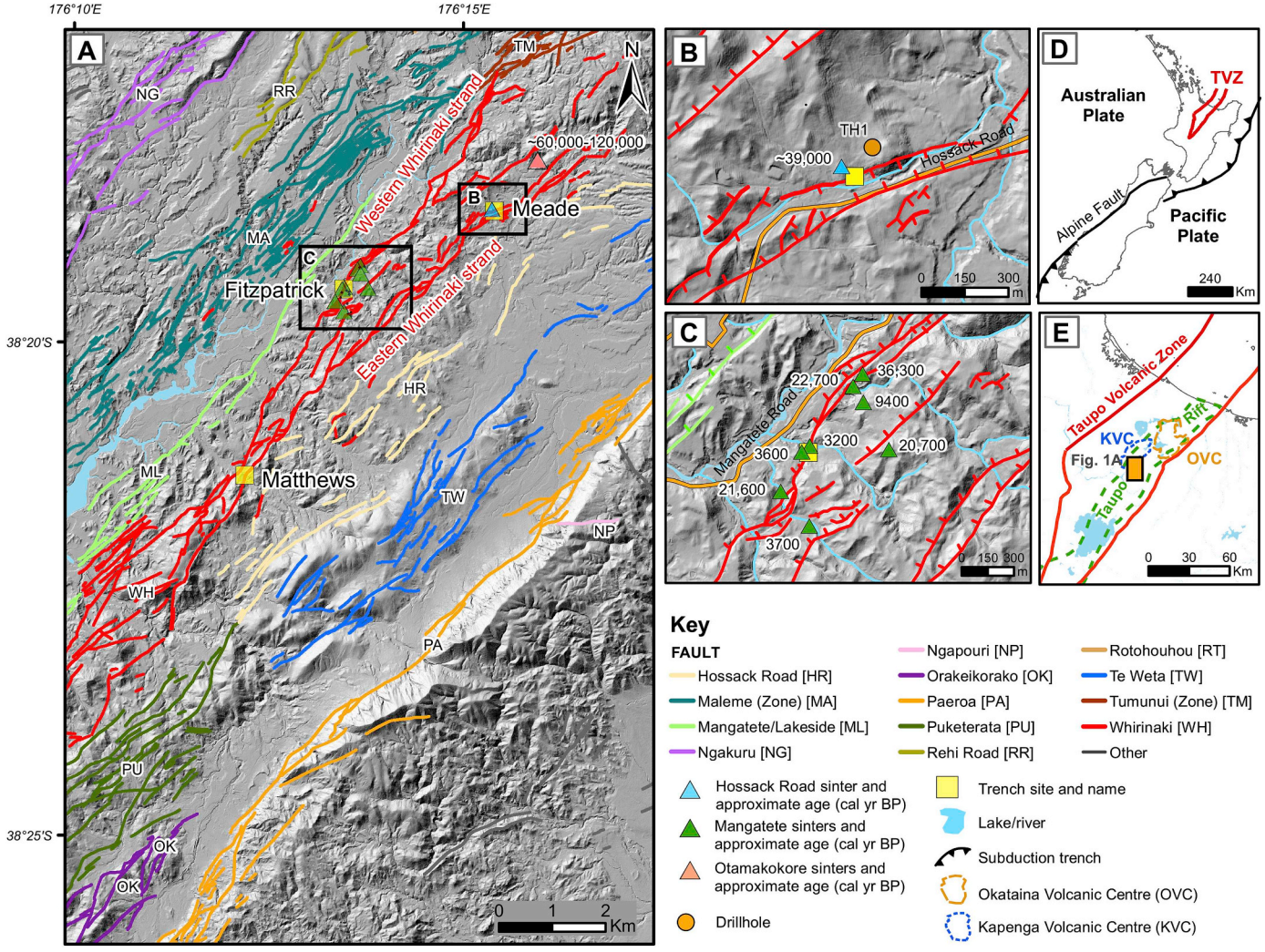

Fig. 1. Location of the study area in central North Island, New Zealand, and newly mapped main faults. **A** DEM of part of the Ngakuru Graben and location of the Meade trench and sinter of this study, and the locations of the Fitzpatrick and Matthews trenches of Canora-Catalán et al. (2008). Locations of the Mangatete sinters (Drake et al., 2014), and the Otamakokore sinters (Holland 2000), are also shown. **B** Location of the Meade trench and sinter and ages (cal. yr BP) with detail of local faults. **C** Location of the Fitzpatrick trench (from Canora-Catalán et al. 2008) and ages (cal. yr BP) of the Mangatete sinters (from Drake et al., 2014) with local fault detail. **D** New Zealand general plate tectonic setting (after Leonard et al., 2010) and location of the Taupo Volcanic Zone (TVZ; Wilson et al., 1995). **E** Context map of the study area (the orange box represents Fig. 1A) within the Taupo Volcanic Zone. The Taupo Rift delineation is from Mouslopoulou et al. (2007); the locations of the Okataina (OVC) and Kapenga (KVC) volcanic centres are from Cole et al. (2014; see also Fig. 13, below). (For interpretation of the references to colour in this figure legend, the reader is referred to the Web version of this article.)

oversaturated geothermal fluids are discharged and cooled at the ground surface (Preston et al., 2008). On the west strand of the Whirinaki Fault, ~3 km southwest of the Meade site (Fig. 1), sinters at Mangatete (near Fitzpatrick site, Fig. 1A and C), c. 36 to 3 cal. ka in age, are exposed on terraces at different elevations, and in association with a debris-flow breccia and hydrothermal-eruption breccias (Drake et al., 2014). The Mangatete sinters exhibit a variety of lithofacies indicative of a range of paleoenvironments and fluid types. Drake et al. (2014) proposed that paleohydrothermal activity in the Ngakuru Graben is related to enhanced permeability caused by faulting, as well as magmatism, during the past c. 60 cal. kyr.

Holland (2000) mapped and sampled several siliceous sinter deposits in the area around Hossack Road, namely the Omatokokore sinters (Fig. 1A). These were tentatively dated to between 160 ka and 60 cal ka based on the stratigraphic juxtapositions of the Ohakuri Formation and (purportedly) Kawakawa tephra. We note that the age of '60 ka' as reported is inconsistent with the age of c. 25.4 cal. ka that should normally be associated with Kawakawa tephra, assuming it was correctly identified by Holland (2000) (alternatively, the age may be approximately correct but pertains to an occurrence of Rotoiti tephra, now dated at c. 50 cal. ka).

Sinters observed at the Meade site appeared to be similar to some of the types found at Mangatete. Sinter units from the trench, the focus of our study, have thin, wavy grey laminae (Fig. 3A and B) and round, pore-like structures frequently containing infilled material in a concentric radial pattern. These resemble the domal stromatolitic type of sinter described by Drake et al. (2014) that are inferred to have formed from near-neutral-pH alkali chloride springs in a mid-apron pool of at least 1 m depth and at temperatures of ~45–55 °C. Sinters exposed in an outcrop on the shoulder-slope of a hill ~410 m above sea level and

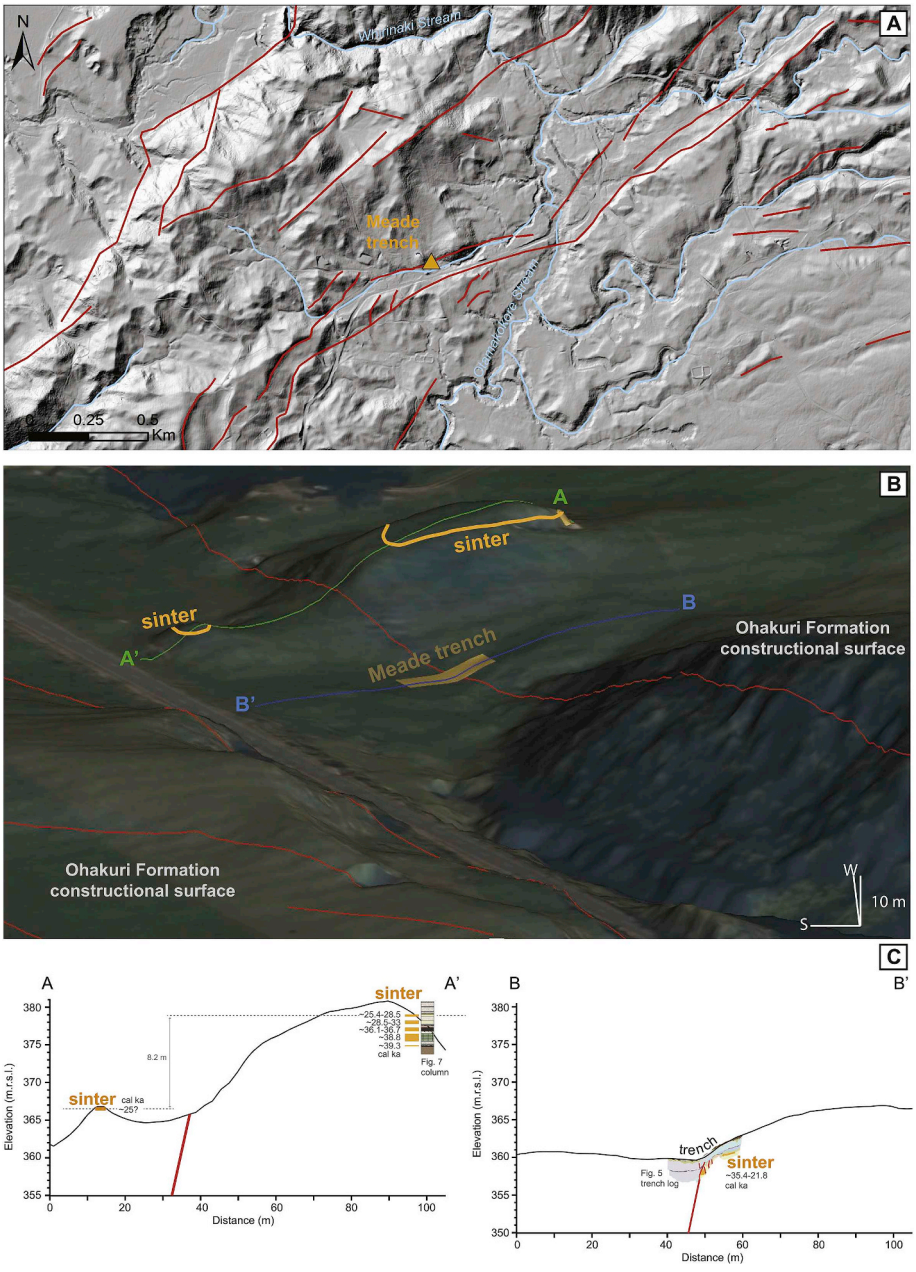

Fig. 2. **A** Location of the Meade trench in relation to the surrounding landscape depicted using a DEM. Main streams and drainage systems are shown in blue, faults in red. **B** LiDAR-derived DEM showing location of the Whirinaki Fault (red line), sinter outcrops, and positions of topographic profiles (2x exaggeration) across the hillside outcrop and trench. **C** Topographic profiles A – A′ and B – B'. The profiles also show an abbreviated stratigraphy at the hilltop shoulder-slope (near A′) and in the trench. (For interpretation of the references to colour in this figure legend, the reader is referred to the Web version of this article.)

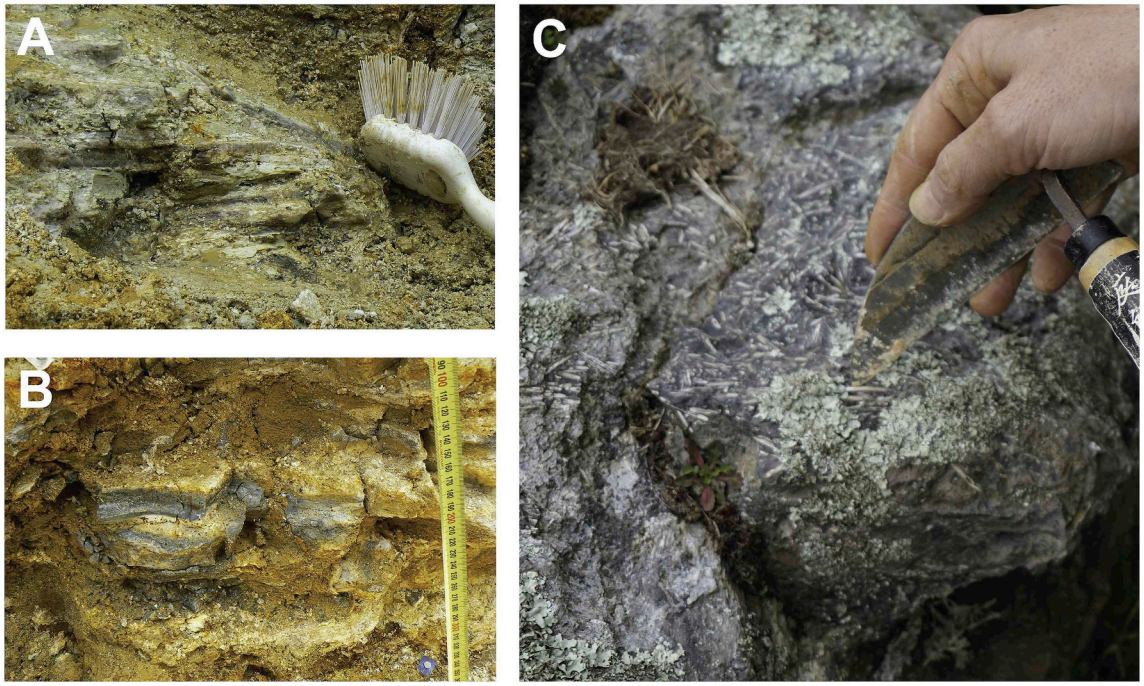

Fig. 3. Types of silica sinters at the Meade site. **A** Wavy grey and white laminated (domal stromatolitic) sinter in the northeast wall of the Meade trench. **B** Wavy grey and white (domal stromatolitic) sinter in the southwest wall of the Meade trench. **C** Plant-rich sinter cropping out close to the site of the Meade trench.

~50 m northwest of the trench show similarities with the plant-rich sinters described by Drake et al. (2014), containing many twigs and silicified reeds in random to subparallel orientations (Fig. 3C).

2. Methods

2.1. Active fault mapping

Previous fault mapping relied on vintage (1940–1965) aerial photography and field measurements (Canora-Catalán et al. 2008; Villamor et al., 2010). Our study improves upon the earlier mapping by integrating more precise fault locations as well as identifying new faults and fault strands by using a high-resolution DEM. The bare-earth DEM, cell size 2 m, was calculated from ground returns collected during an aerial LiDAR survey commissioned by the Bay of Plenty Regional Council as part of the BOPLASS project 2010 (BOPLASS, 2013). The DEM and derived products (e.g., hillshade and slope models) were visually analysed in a GIS and the location of active traces of the Whirinaki Fault identified, reviewed, and mapped from their geomorphic expression, i.e., the identification of fault scarps that displace young landscape surfaces. In this case, the Whirinaki Fault displaces formations and surfaces with ages ranging from c. 240 ka to 1.7 cal ka (Nairn, 2002; Leonard et al., 2010).

2.2. Paleoseismic trenching

A north-west–south-east aligned double-bench style paleoseismic trench was excavated across the north section of the east strand of the Whirinaki Fault on the Meade property on Hossack Road, Ngakuru (Fig. 1B), at grid reference U16/1884881, 5754914 (New Zealand Transverse Mercator). The trench measured 23 m in length, 5 m in width, and 3 m in depth, with benches up to 1.5 m deep at the deepest end. Two cores, 1.2 m and 1.1 m long, were extracted using a vibrocorer from below the floor of the trench on either side of the exposed fault to examine the sub-trench stratigraphy. The stratigraphy and deformation in the trench, including the superpositions and physical properties of tephras and buried soils, were described, measured, and logged onto drafting paper using a 1 × 1 m reference grid. Further detail on the methods associated with paleoseismic trenching is available in McCalpin (2009).

2.3. Tephra sampling/processing, ferromagnesian mineralogy, and electron microprobe analysis of glass shards

After the trench walls were cleaned back to expose a fresh face, samples of tephra deposits were taken from the upper and lower parts of each unit. Each sample was wet sieved and the 63–250 μm fraction retained. Vertical and tilted Franz electromagnetic separators were used to isolate ferromagnesian minerals from volcanic glass shards and felsic minerals (Froggatt and Gosson, 1982). To examine ferromagnesian mineralogical assemblages, temporary mounts were made using welled (dual cavity) slides, with loose ferromagnesian mineral grains (crystals) suspended in clove oil. The minerals were identified on the basis of their optical properties under a polarizing microscope, counted, and tabulated for later comparison.

The glass shards were mounted in resin blocks, polished, and coated in carbon prior to their analysis for major elemental composition (the procedure is described in Lowe, 2011; Hall and Hayward, 2014). Electron probe microanalysis (EPMA) was conducted using the JEOL JXA-8200 SuperProbe at Victoria University of Wellington, operating with a beam diameter of 10 μm, beam voltage of 15 kV, and probe current of 8 Å, with asynchronous measurement and ZAF correction on oxides. Peak and background count times for each element were 30 s and 15 s, respectively, except for Na, for which peak and background count times were each 10 s (Kuehn et al., 2011; Pearce et al., 2014). The standards used were ATHO-G rhyolitic glass (Jochum et al., 2006) and VG-568 rhyolitic glass (Jarosewich et al., 1980). Typically, at least 20 shards were analysed from each tephra sample. The resultant glass analyses, reported as oxides, were normalised (following Lowe et al., 2017) in Excel and plotted using GCDkit 4.1, an open-source software package written in R language for use in igneous petrology (Janoušek et al., 2006, 2011).

2.4. Radiocarbon dating

Silica sinter at ~5-m depth in the outcrop on the shoulder of the hill adjacent to the trench was sampled and dated using accelerator mass spectrometry after various pre-treatments. Four samples of sinter were soaked in hydrogen peroxide to oxidize exterior organic contamination and then washed with distilled water. These samples were crushed and treated with hot hydrochloric acid (10%), then washed three times with distilled water. The samples were then digested in hydrofluoric acid (50%) and allowed to sit for several days, fresh hydrofluoric acid being added as required. The dissolved residue was washed three times with hot hydrochloric acid (10%), then twice with distilled water, before being centrifuged and filtered at 155 μm. Almost all material went through the 155 μm sieve. The > 155 μm material was examined under a microscope, seen to comprise colourless quartz grains, and hence was discarded. The < 155 μm material was sieved at 6 μm, with the < 6 μm material discarded, and the > 6 μm material collected in centrifuge tubes. Sodium polytungstate with a density of 1.9 g/ml was used to separate minerals and float plant material. The collected plant material was checked under a microscope and found to contain some pollen and plant cell wall material. This plant microfossil material was photographed and loaded into a combustion tube and combusted to CO_2 in evacuated quartz tubes with copper oxide and silver wire. The carbon content of the combusted fractions from each of these sinters was > 40%, confirming that the primary component in the fractions was cellulose. The CO_2 was reduced with H_2 over an iron catalyst and the resulting graphite was analysed in the EN tandem accelerator at the Rafter Radiocarbon Laboratory at GNS Science's National Isotope Centre, Lower Hutt, New Zealand.

2.5. Trench restoration

The deformation observed on the faults in the trench was restored in a similar fashion to that described by Villamor and Berryman (2006) and Berryman et al. (2008). Trench restoration is a form of analysis which involves removing the deformation produced by each rupture event consecutively. The method includes removing the slip along the fault and possible drag folding to juxtapose the same unit across the fault. Because of erosion of the footwall and mantling of tephra-fall deposits in between rupturing events, the original layers do not tend to be horizontal. It is thus important to reconstruct the original thickness and geometry of each stratigraphic unit. The restoration is undertaken in stages (for each rupturing event) and the amount of displacement and degree of unit rotation is recorded as the analysis progresses. Restoration can be used to calculate the single event displacement (henceforth SED) associated with each event and its timing. In volcanic regions, it can also be used to assess time associations between volcanic events, fault rupture events, and, in our case, hydrothermal events that generated silica sinter.

In a previous study on the Whirinaki Fault, Canora-Catalán et al. (2008) used trench restoration to obtain estimates for the SEDs, recurrence intervals, and slip rates on two individual fault strands: the south section of the eastern strand (Matthews trench) and the north section of the western strand (Fitzpatrick trench) (Fig. 1). Adobe Illustrator was used to perform the detailed graphical restoration of deformation in the Meade trench, following protocols given in the data supplements of Villamor and Berryman (2006) and Villamor et al. (2011) and from Berryman et al. (2008). Each step of the restoration was recorded, including the number of events restored, the active fault planes on which the deformation occurred, the amount of deformation associated with each event restored (a SED), and the timing of the event as determined by the ages for the bracketing tephra deposits. Uncertainties of the SED estimates are based on the range of displacement needed for restoration that still match the original scarp pre-event. For well-defined layer contacts, and based on the technique used to produce the trench log (manual grid) and the scale of the map (1: 20), the error value is ~0.2 m.

2.6. Fault parameters: slip rate and rupture recurrence interval

Fault slip rate has been produced by accumulating SEDs from individual fault restorations and the age of the restored units (together with their respective uncertainties). The slip rates are visualised in displacement/time plots and compared with those from other trenches on the Whirinaki Fault.

The average recurrence interval of ruptures (T) is calculated using the formula

$$T = N/n$$

where N is the number of years in the time period in question, and n is the number of rupture events recorded within that timeframe. Recurrence intervals have also been estimated as the time in between individual events for the event history in the trench.

3. Results

3.1. Active fault traces of the Whirinaki Fault

The new mapping of the Whirinaki Fault (Fig. 1) does not differ dramatically from that of Canora-Catalán et al. (2008). However, it does provide more detail to spatially relate the paleohydrothermal features to different parts of the fault. The western and eastern strands of the fault are 1 km apart at the surface, except in the vicinity of the Matthews trenches where they are separated by only 200 m. North of the Matthews trench (sited on the western fault strand; Canora-Catalán et al. 2008), the western strand strikes 035° and dips to the northeast. The Mangatete sinters and the Fitzpatrick trench of Canora-Catalán et al. (2008) are located on the eastern strand (Fig. 1C). The eastern fault strand strikes at ~045° (a typical strike for this part of the rift) and has a northwest dip up to 200 m south of the Meade site. At that location the strike changes to 060° and the fault splays into two faults that form a narrow graben. The Meade trench (this study) and fossil sinter deposits are located on the northeast splay within the narrow graben, on the fault from the splay that dips southeast (Fig. 1B).

3.2. The Meade site

The Meade site is located in hilly land 15 km south of the currently active OVC (Fig. 3). The hills are underlain by 240-ka-old ignimbrite of the Ohakuri Formation, which was erupted from Ohakuri Caldera (Gravley et al., 2006, 2007; Leonard et al., 2010; see also Fig. 13, below). The fossil sinter studied here is exposed on a farm track close to the top of one of the hills (point A in Fig. 2B) on the upthrown side of the fault, and ~8–12 m above the valley floor. A small hill in the downthrown side has restricted exposures of sinter that we assume to be correlative to the sinter studied here (Point A' in Fig. 2B). The trench was sited across the fault and on the valley floor where the scarp, approximately 5.5 m high, was of an appropriate height for excavation of paleoseismic trenches. Fossil sinter was also exposed in the trench (see below).

Near the Meade trench, an exploration mineral well (TH1; Fig. 1B) was drilled in 1988 to investigate the fossil hydrothermal system at this location (Alder and Sharp, 1988). A hydrothermal vent breccia ~40 m thick is intersected by the drillhole, overlain by a disrupted sinter sheet.

3.3. Tephra identification in the Meade trench

Tephra correlations were determined largely based on a combination of stratigraphic position, physical properties, ferromagnesian mineralogical assemblages, and glass-shard major element compositions (Lowe, 2011). However, neither Kaharoa nor Taupo tephras was analysed geochemically because their distinctive physical properties and

their surface or near-surface positions, respectively, meant they could be easily identified with confidence in the field. Furthermore, Kaharoa pumice clasts contained biotite (identifiable in the field), a key marker mineral associated with this tephra (Lowe et al., 1998, 2008; Nairn, 2002).

The dominance of pyroxene in Taupo tephra, and the presence of cummingtonite in Rotoma Tephra and of biotite in Rotorua and Okareka tephras, are consistent with previous ferromagnesian mineralogical data associated with these tephras (Table 1; Lowe et al., 2008). In addition, the major element glass compositions for the Rotoma, Rotorua, and Okareka tephras at Meade trench (Fig. 4) essentially match those reported for the same tephras by Lowe et al. (2008), indicating that they are correlatives. That each of these three tephras has probably derived from more than one magma type (e.g., see Smith et al., 2005; Lowe et al., 2008; Shane et al., 2008) is evident in the glass-shard major element data presented here. For example, the analyses of glass from Rotorua tephra plot in two distinct populations (Fig. 4C and D), indicating that this tephra at Meade trench comprises eruptives of both magma types and thus probably represents their intermingling (Smith et al., 2004; Loame, 2016).

3.4. General stratigraphy and ages of the Meade trench

The generalised stratigraphy of the trench units, including ages, is presented in Fig. 5. It comprises, from top to bottom, Kaharoa, Taupo, Rotoma, Rotorua, and Okareka tephras overlying domal stromatolitic sinter, volcanogenic sediments (denoted as Hinuera Formation), an older domal stromatolitic sinter, and variably-weathered ignimbrite of the Ohakuri Formation. The tephras have well-established ages derived from dendrochronology and radiocarbon dating using both wiggle-matching and Bayesian age-depth modelling (Table 2). The Hinuera Formation in the region generally comprises laminated, commonly cross-bedded fluvial sands and gravels dominated by clasts of pumice and ash together with felsic crystals and rhyolite lithics, the younger part of the formation being derived predominantly from reworking of the Oruanui Formation (Vucetich and Pullar, 1969; Manville and Wilson, 2004; Leonard et al., 2010), equivalent in age to Kawakawa tephra, aged c. 25,400 cal. yr BP (Vandergoes et al., 2013). We suggest therefore that an age between c. 25.4 cal. ka and c. 21.8 cal. ka very likely applies to the Hinuera Formation sediments and the encapsulating sinters evident in the Meade trench (Fig. 5). On this basis, there is an unconformity, probably erosional, between the lowermost sinter and the ignimbrite of the Ohakuri Formation.

Soil horizon development was evident in the upper parts of the tephras (Fig. 5). These now-buried horizons (recorded as paleosols: Lowe and Palmer, 2005) are paraconformities that represent volcanic quiescence.

3.5. Detailed stratigraphic and structural architecture of the Meade trench

In the northern part of the trench (foot wall), there is a succession of weakly weathered late Quaternary-age tephras (Okareka, Rotorua, Rotoma) overlying volcanogenic sediments of the Hinuera Formation and/or the Ohakuri Formation (Figs. 5 and 6, and Fig. S1 in Supplementary data). Thin deposits of Taupo lapilli (equivalent to subunit Y5 of Wilson, 1993) and Rotongaio ash (subunit Y4) (collectively referred to as Taupo tephra; see Wilson and Walker, 1985; Froggatt and Lowe, 1990), and Kaharoa tephra, cap the sequence.

In the southern part of the trench (hanging wall), the Taupo tephra is dominant, with up to 2.5 m of (non-welded) Taupo ignimbrite (subunit Y7 of Wilson, 1985, 1993) exposed in the deepest part of the trench and only relatively thin (< 0.5 m) late Quaternary tephras that include Okareka and Rotorua tephras. Cores taken from the deepest part of the trench showed reduced thicknesses of late Quaternary tephras (mainly Okareka and Rotorua) and, at the base, c. 0.5 m of fine to medium sandy deposits uncorrelatable with other units observed in the trench.

Fault deformation is visible in the trench, affecting all of the deposits from the Ohakuri Formation to Taupo tephra. Deposits younger than Taupo are not faulted. Close to the midpoint of the trench, and more prominent on the southwest wall, are siliceous sinters and a highly mixed zone of brecciated and sheared materials, much of which comprises fragments of siliceous sinter (Fig. 7) sheared upwards along the hanging wall of the fault plane. The fault associated with the shear zone has a strike/dip of 025/69 northwest, whereas most of the other faults and fractures along the southwest wall close to the shear zone are dipping to the southeast in the opposite direction and have a strike greater than 040°.

3.6. Contrasting stratigraphy of deposits in section on adjacent hill and their chronology

The section on the shoulder-slope of the adjacent hill comprises a sequence of tephra layers, including five additional to those identified in the trench, namely Kawakawa, Poihipi, Hauparu, Te Mahoe, and Tahuna tephras, together with one uncorrelated tephra, siliceous sinters, and other deposits and paleosols (Fig. 8; sources of ages are in Table 2). Most of these older tephras were identified using the same criteria used to correlate the tephras in the Meade trench (Loame, 2016). The pink pumice clasts (Hauparu) and the accretionary lapilli and abundant lithics (Te Mahoe) are key diagnostic physical properties for these two tephras (Jurado-Chichay and Walker, 2000; Shane et al., 2005). Although not used for reconstructing the history of fault rupturing, the older tephras provide chronological constraints for sinter development on the hill, especially the Tahuna tephra, which is interbedded with sinter (Fig. 8). The identification of the Tahuna tephra in the hill section was therefore especially important, with selected major elements in glass shards showing they closely matched equivalent analyses for this tephra reported in the literature (Fig. 4G and H), thus confirming its correlation.

The mean age on the entrained plant material collected from within the sinter at ~5-m depth is 34,360 ± 460 ^{14}C yr BP (NZA33105), calibrated at 95% probability range to 38,870 ± 1106 cal. yr BP using SHCAL13 (Hogg et al., 2013). This age, on material immediately above Tahuna tephra, is consistent with a previous age of 39,268 ± 2386 cal yr BP (n = 2) reported by Molloy et al. (2009) for Tahuna tephra in Auckland maar deposits (cf. somewhat younger ages derived from optical dating reported by Lian and Shane, 2000). In turn, the presence of Te Mahoe tephra (c. 36.7 cal. ka) and Hauparu tephra

Table 1
Generalised ferromagnesian mineral assemblages[1] of samples from the Meade trench compared with data for Taupo, Rotoma, Rotorua, and Okareka tephras from Froggatt and Lowe (1990) and Smith et al. (2005).

Tephra name	Meade samples	Froggatt and Lowe (1990)	Smith et al. (2005)
Taupo	cpx > opx > fe-ti + hbl	opx + cpx + hbl	opx > fe-ti > cpx
Rotoma	opx > fe-ti > cgt > hbl	opx + cgt ± hbl	opx + hbl ± cgt ± bi > fe-ti
Rotorua	bi > opx > fe-ti + hbl	opx + hbl + bi ± cpx	bi > hbl > fe-ti > opx
Okareka	fe-ti > opx > hbl > bi + cgt	opx + hbl + bi	opx + hbl ± cgt ± bi > fe-ti

[1]Abbreviations: opx, orthopyroxene (mainly hypersthene); cpx, clinopyroxene (mainly augite); hbl, hornblende; cgt, cummingtonite; bi, biotite; fe-ti, iron-titanium oxide (mainly titanomagnetite).

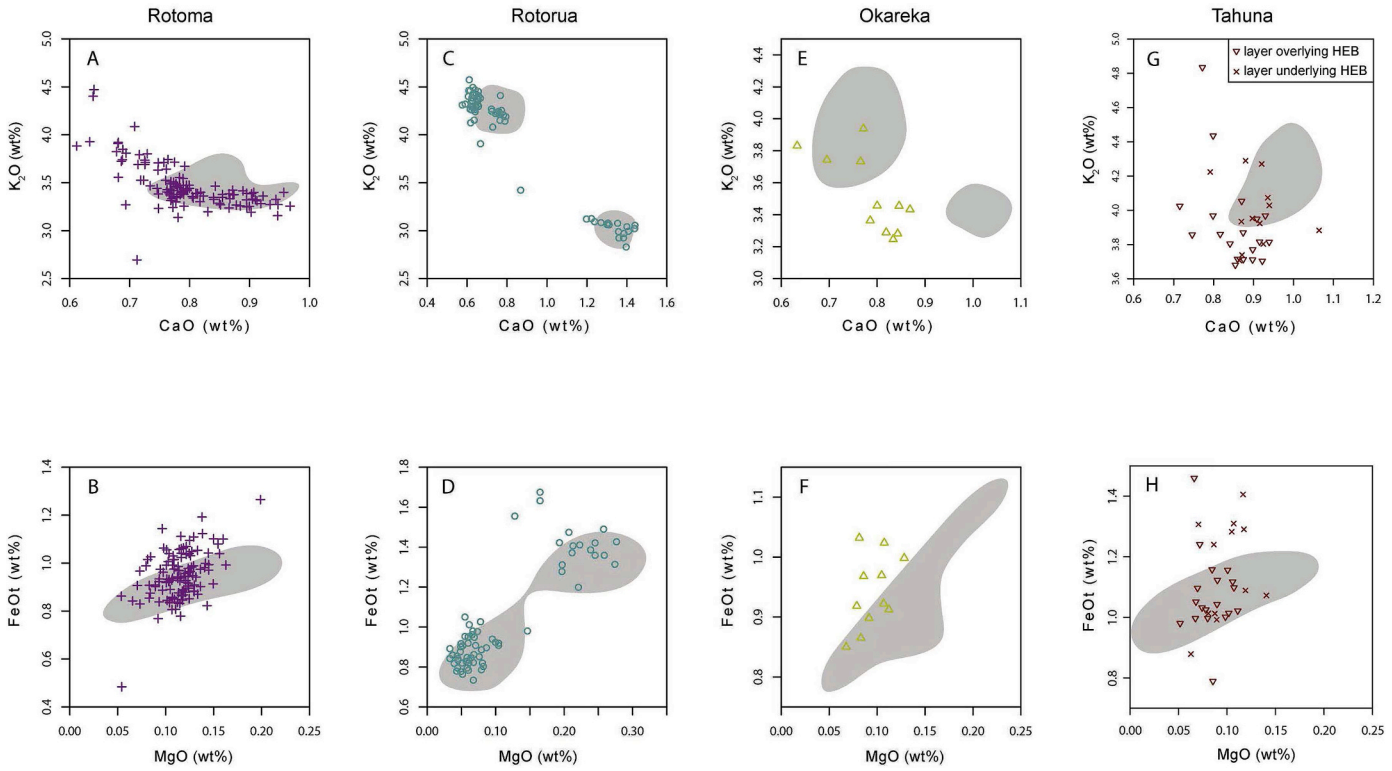

Fig. 4. Bivariate plots of K_2O-CaO (A-C-E-G) and FeOt-MgO (B-D-F-H) (normalised data) for individual glass shards of representative samples from Rotoma, Rotorua, and Okareka tephras in the Meade trench, and Tahuna tephra immediately above and below the hydrothermal eruption breccia (HEB) on the hillside outcrop (see Fig. 8 below). Grey polygons show range of data for glass analyses of the same tephras from Lowe et al. (2008); the polygon for Tahuna tephra includes data from Smith and Shane (2002). Total iron expressed as FeOt.

(c. 36.1 cal. ka) in the stratigraphic sequence (Fig. 8) lends further support to the chronology we have established.

Using tephra layers and other features as tie points, we have correlated some of the stratigraphic units exposed in the hill section with those in the fault footwall at the trench site (Fig. 9).

3.7. Trench restoration

The progressive displacement in the southwest wall of the trench is displayed in Fig. 10. Four occurrences of SEDs were recorded and designated as Meade-Hossack events (MH1 to 4, from younger to older) (Table 3). Note that although we are naming these as SEDs, some of them could be produced by more than one rupture (see more discussion below). MH1 resulted in an SED of 0.55 m, occurring after Taupo tephra (c. 1.7 cal. ka) and before Kaharoa tephra (Fig. 10B). MH2 resulted in an SED of 0.85 m, occurring after Rotoma tephra (c. 9.4 cal. ka) and before Taupo Tephra (Fig. 10C). MH3 resulted in an SED of 1.2 m, occurring after Rotorua tephra (c. 15.6 cal. ka) and before Rotoma tephra (Fig. 10D). MH4 resulted in an SED of 2.4 m, occurring after the deposition of Hinuera Formation sediments (< c. 25.4 cal. ka) and before deposition of the Okareka tephra (c. 21.8 cal ka; Fig. 10E). A fifth event, MH5, was observed but is too poorly constrained to be useful, occurring between the deposition of Ohakuri Formation (c. 240 ka) and the Hinuera Formation, and the displacement is difficult to measure because the base of the Ohakuri Formation is not visible and therefore cannot be restored. However, we have been able to measure the geomorphic offset of the sinter on the shoulder-slope of the adjacent hill (hilltop sinter; c. 25–28 cal. ka) with a displacement of ~8.2 m (Fig. 2C; Table 3).

3.8. Slip rates

The slip rates for the Whirinaki Fault estimated for the Meade site are shown in Fig. 11, along with comparative data pertaining to the Matthews and Fitzpatrick trenches, and in Table 3. A uniform probability distribution has been assumed when dealing with uncertainties. The slip rates for the different time periods are based on incremental displacement and the constraining ages for each event (each displacement increment is an event). Slip rates were calculated for each increment in displacement and we used the constraining ages for this displacement. For example, MH3 uses the mean ages of the constraining Rotorua and Rotoma tephras, at 15.6 and 9.4 cal. ka, respectively. The displacement for this event is 1.2 m, giving a mean slip rate of 0.097 ± 0.016 mm/yr.

If our assumption of the age of the geomorphic surface on the downthrown side of the hill is correct, the fault slip rate is in the range of ~2.6–0.1 mm/yr for the time span between the sinter in the outcrop at the top of the hill (c. 28.4 cal. ka) and that of Okareka tephra (c. 21.8 cal. ka). The age for the Hinuera Formation involved in ~4 m of displacement (cumulative for four events) in the Meade trench is uncertain as we do not have an age for the base of the Hinuera Formation exposed in the trench. However, it is probable that the valley incision, and subsequent deposition of Hinuera Formation, occurred after the sinter on the hillside ceased precipitating because it would likely be hydrologically more difficult for sinter to be deposited on the hillside (backslope) if the valley existed (although we acknowledge this is an assumption, cf. Rimstidt and Cole, 1983). Therefore, we have used the youngest age of Hinuera Formation suggested for this area (i.e., younger than Kawakawa tephra, which is c. 25.4 cal. ka). From the time of deposition of the Okareka tephra (c. 21.8 cal. ka) to deposition of Taupo tephra (c. 1.7 cal. ka), the slip rate seems to decrease to values of ~0.1–0.6 mm/yr. The slip rate from the present to Taupo tephra time is not representative because the earthquake cycle is incomplete.

The mean long-term slip rate for the Whirinaki Fault at the Meade trench for the late Quaternary (i.e., since the end of deposition of the

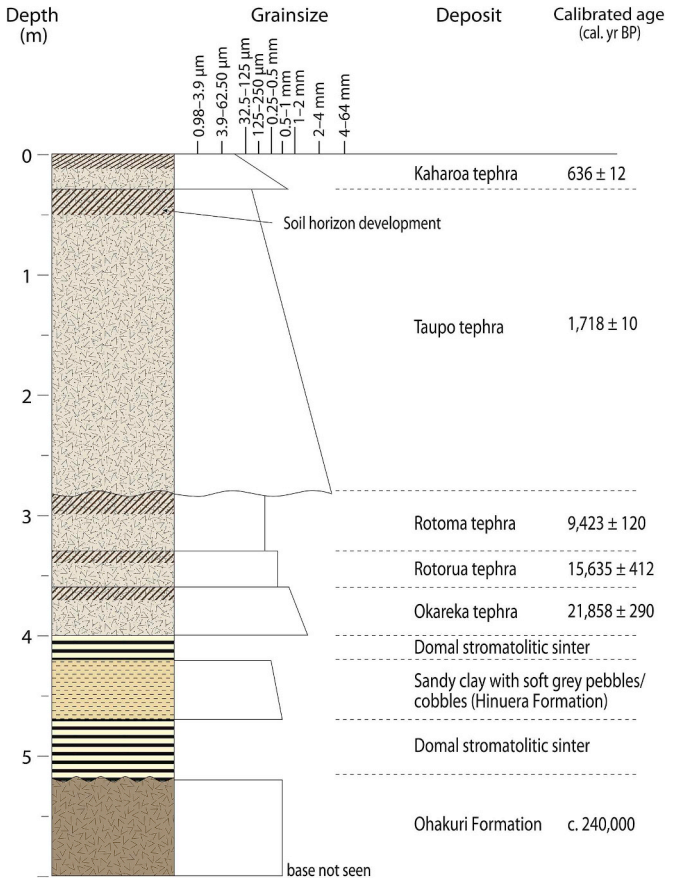

Fig. 5. General stratigraphy of the Meade trench and ages of tephras and other deposits. Paleosols occur in the upper parts of each tephra; modern soil horizons are formed on Kaharoa tephra. Grain sizes depicted are from field observations. Ages are from sources listed in Table 2. The sediments of the Hinuera Formation are assumed to be aged between c. 25.4 cal. ka (i.e., younger than Kawakawa tephra/Oruanui Formation) and c. 21.8 cal. ka (Okareka tephra).

Hinuera Formation c. 21.8 cal. ka) is 0.28 ± 0.04 mm/yr.

3.9. Rupture recurrence interval

Trench restorations for the Meade trench are better constrained for the last three events, MH1 to MH3 (Fig. 10B, C, and D) than for the older event (MH4, Fig. 10E). However, constraining the inter-seismic interval (or time between consecutive rupturing events) is difficult because, in the Meade trench, the bracketing ages (derived from the known tephra ages, which are expressed as 95%-probability ranges; Table 2) for the events are the same for the youngest possible age of one event and the oldest of the next event in most cases. In these cases, the events could have occurred close in time (just before and after the bracketing tephra) or with a large inter-seismic interval. Maximum inter-seismic intervals are 8,923 years for interval between MH1 and MH2, 14,339 years for interval between MH2 and MH3, and 16,217 years for interval between MH3 and MH4. These intervals are estimated using the oldest likely age of the earlier event and youngest likely age of the later event (e.g., the maximum inter-seismic interval for MH1-MH2 is calculated using the youngest age for Kaharoa tephra and the oldest age for Rotoma tephra). Only for the inter-seismic interval MH3-MH4 can we calculate a minimum value of 5,521 years. It is important to note that if one of the inter-seismic intervals were to have one of the maximum values above, the other intervals would need to be smaller, and thus the recurrence intervals will vary in time. A large SED of 2.4 m for MH4 suggests that the displacement is likely to have been accommodated in more than one event. In that case, the inter-seismic interval between the "two MH4 events" could be of a maximum of 3,000 to 4,000 years. Another way to look at the rupture recurrence interval is through an average value. In this scenario, for the period since ~25,520 (oldest likely age of Kawakawa tephra), average values of 6,380 years (for 4 events) or 5,100 years (for 5 events) are able to be calculated.

Table 2
Tephra-fall deposits and ignimbrites (Taupo ignimbrite; Ohakuri Formation) identified in the Meade trench and in the adjacent hill section, and their ages.

Tephra or ignimbrite (and source volcano[a])	Calibrated age (cal. yr BP)
Kaharoa Tephra[b] (OVC)	636 ± 12
Taupo Tephra[c] (TVC)	1718 ± 10
Rotoma Tephra[d] (OVC)	9423 ± 120
Rotorua Tephra[d] (OVC)	15,635 ± 412
Okareka Tephra[e] (OVC)	21,858 ± 290
Kawakawa Tephra[e,f] (TVC)	25,358 ± 162
Poihipi Tephra[e] (TVC)	28,446 ± 670
Hauparu Tephra (Unit F, MSg)[g] (OVC)	c. 36,100
Te Mahoe (Unit E, MSg)[g,h] (OVC)	c. 36,700
Tahuna Tephra[i] (TVC)	39,268 ± 2386
Ohakuri Formation[j] (OHC)	c. 240,000

[a] OVC, Okataina Volcanic Centre; TVC, Taupo Volcanic Centre; OHC, Ohakuri caldera (after Leonard et al., 2010).
[b] Radiocarbon wiggle-match calendrical date (on tree-ring sequence) of 1314 ± 12 AD (95% probability range, PR) from Hogg et al. (2003).
[c] Radiocarbon wiggle-match calendrical date (on tree-ring sequence) of 232 ± 10 AD (95% PR) from Hogg et al. (2012).
[d] Calibrated radiocarbon age (95% PR) from Bayesian flexible-depositional age modelling from Lowe et al. (2013).
[e] Calibrated radiocarbon age (95% PR) from Bayesian Tau_boundary-function modelling (OxCal) from Lowe et al. (2013).
[f] Calibrated radiocarbon age (95% PR) from Bayesian Tau_boundary-function modelling (OxCal) from Vandergoes et al. (2013). Dunbar et al. (2017) reported an ice-core-based age of 25,318 ± 250 cal. yr BP (± 2 sd) for Kawakawa/Oruanui tephra.
[g] Estimated calibrated age from Smith et al. (2005). MSg = Mangaone Subgroup (Jurado-Chichay and Walker, 2000).
[h] Jurado-Chichay and Walker (2000) reported a single radiocarbon age 31,720 ± 370 ^{14}C yr BP on Te Mahoe tephra. Calibrating this age using OxCal v4.3.2 (Bronk Ramsey, 2009) and SHCal13 (Hogg et al., 2013) gave an age of 35,575 ± 746 cal. yr BP (95% PR). Two imprecise radiocarbon ages on Hauparu tephra, of limited value, are reported in McGlone et al. (1984) and Froggatt and Lowe (1990).
[i] Calibrated weighted mean radiocarbon age (95% PR) from Molloy et al. (2009, Table DR1).
[j] Rounded age from two Ar/Ar radiometric ages of 240 ± 11 and 244 ± 10 ka (± 1 sd) from Gravley et al. (2006, 2007).

4. Discussion

A summary of events of the past c. 40,000 cal. years is presented in Fig. 12, along with comparisons with other rupture events from the Matthews and Fitzpatrick trenches on the southeast section of the west strand of the Whirinaki Fault studied by Canora-Catalán et al. (2008). Included on the summary diagram, which is based on the tephrostratigraphic framework we have developed, are some of the sinter emplacement intervals observed in the trench and on the upper hillside outcrop at the Meade site, and sinter emplacement intervals on the west strand of the Whirinaki Fault derived from Drake et al. (2014). MH5 has been excluded from the summary figure because of poor temporal constraint (> c. 25.4 cal ka, < c. 240 ka).

4.1. Comparison between rupturing events as evident in trenches along the Whirinaki Fault

On the basis of the active fault mapping, we interpret that both the Matthews and the Meade trenches lie on the same fault strand (Fig. 1).

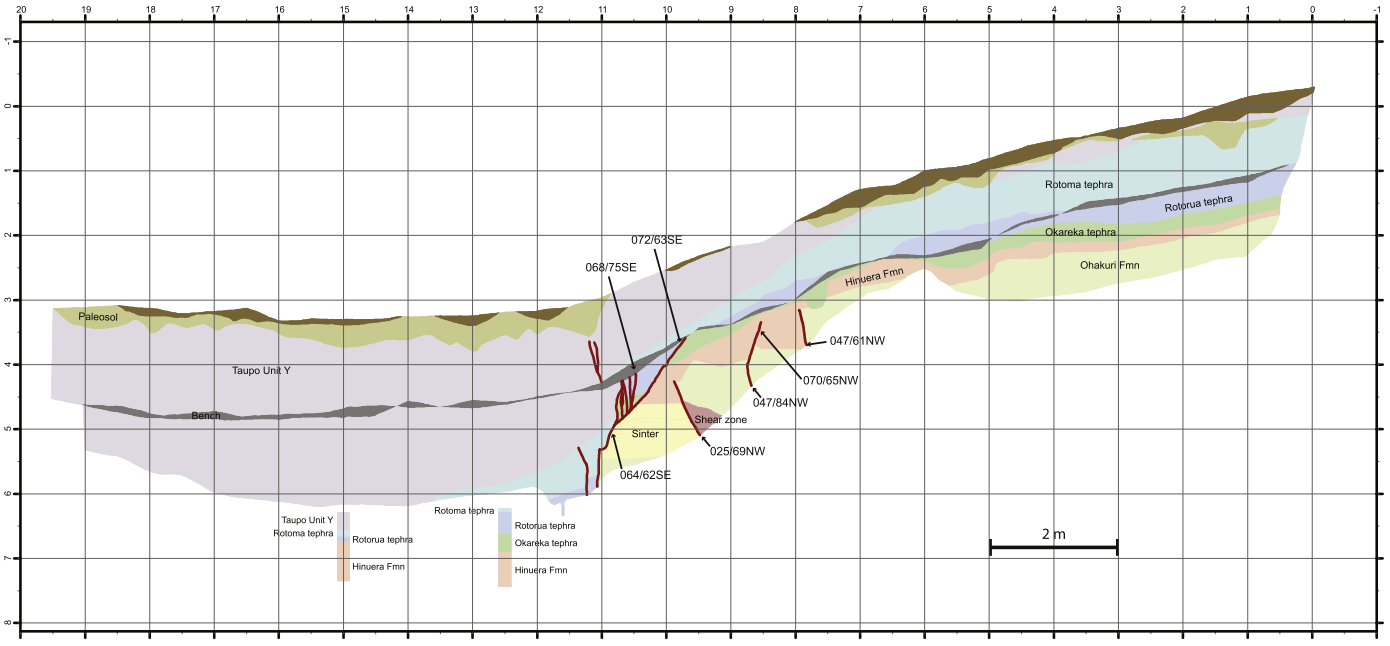

Fig. 6. Trench log for the northern part of the southwest (SW) wall of Meade trench, with named tephras (see text and Fig. 9). Other deposits include sinter, volcanogenic sediments of the Hinuera Formation, and a mixed breccia in the shear zone. Several paleosols are recorded as well.

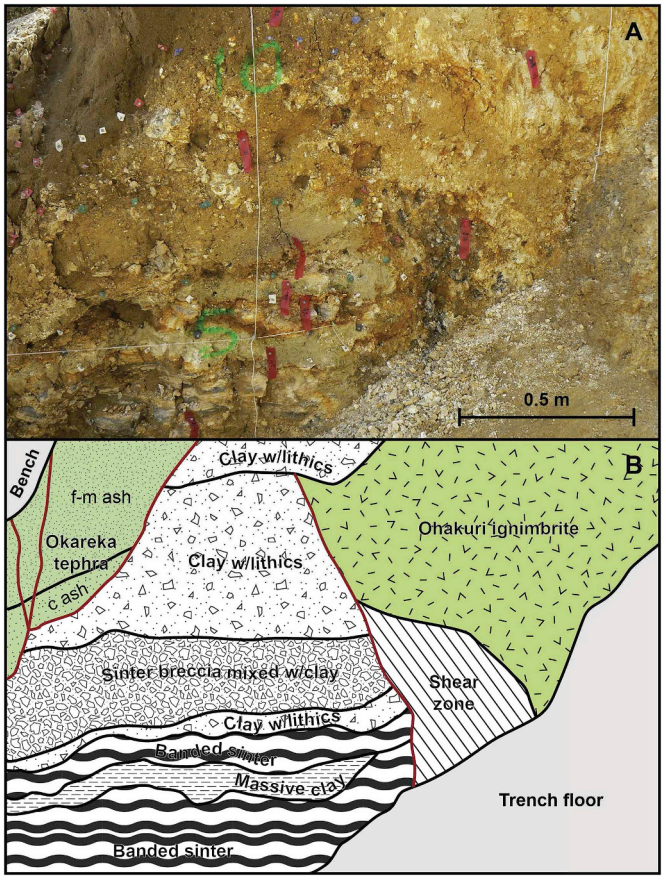

Fig. 7. Further detail of the zone of shear on the southwest wall of Meade trench as shown in Fig. 6. **A** Photograph, and **B**, sketch of fractures and main units. w, with; f-m, fine to medium; c, coarse.

The timing of ruptures in these two trenches temporally coincide for the period between the Kawakawa and Rotoma tephras (Fig. 12; events MH3-M3 and MH4-M4; note that the large SED for event 4 in both trenches is likely to represent more than one event). However, they do not seem to coincide during the period from the time of the Rotoma eruption to the present (events 1 and 2 on both trenches). A possible explanation for the lack of correlation is that rupture of the Whirinaki Fault western strand (Fitzpatrick trench) was transferred to the northern part of the eastern strand (Meade trench) through east-west traces during the most recent period but not to the southern parts (Matthews trench), or that the rupture at Meade trench connected to ruptures farther north (on other faults). Alternatively, ruptures might extend from the Matthews site to the eastern strand of the Whirinaki Fault close to the Meade site, rupturing the southern fault strand of the narrow graben at Hossack Road (Figs. 1B and 2), but this strand has not yet been trenched.

The comparison of event timing from the different trenches on the Whirinaki Fault is short of more trenching studies, but we can suggest that defining permanent rupture segment boundaries for faults on this part of the Taupo Rift (as have been defined in the National Seismic Hazard Model; Stirling et al. 2012) may not fully represent fault behaviour (fault rupture length may vary from event to event). In this region, single event displacements are variable for the same trench site (this study; Berryman et al., 2008; Canora-Catalán et al. 2008; Nicol et al., 2009), supporting the idea that a fault may also rupture with different lengths (and thus different magnitudes). Berryman et al. (2008) have also demonstrated that rupture of a fault that splays into multiple traces on the surface can be apparently random in terms of which traces rupture during each event. Moreover, the complexity (e.g., presence of small transfer faults, fault splays), and the strong physical connectivity of the fault traces that is expressed by the fault map (Fig. 1), could suggest that it is hard to predict which sections of faults may rupture together (i.e., it is difficult to define rupture boundaries).

Despite these limitations, we conclude that it is very probable that some ruptures (e.g., MH3-M3 and MH4-M4) along the Whirinaki Fault may extend to the Meade trench as modelled by Canora-Catalán et al. (2008). The combined fault rupture history also suggests that the western fault strand seems to have been more active (four events and a total of 3.4 m of displacement) since the Rotoma eruption, while the eastern strand has been less active during that time, at least in the middle section (Matthews trench: two very recent events with only 0.7 m of total displacement). The fault activity at the Meade site (northern sector of the eastern strand) seems to have had more constant

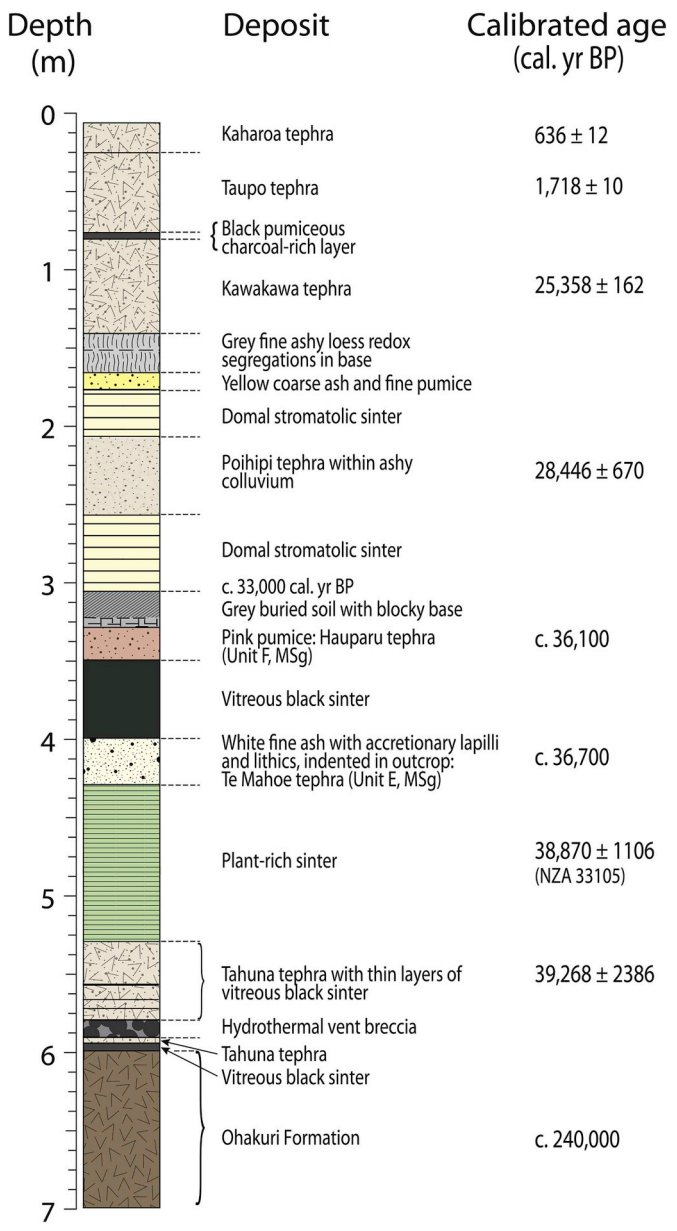

Fig. 8. Stratigraphy of deposits in the hill adjacent to the Meade trench. Ages of the tephras and the basal ignimbrite (Ohakuri Formation) are given in Table 2; the calibrated ^{14}C-age for plant-rich sinter is from this study. The base of the domal stromatolic sinter at ~3 m depth is estimated to be aged c. 33,000 cal. yr BP, assuming that the underlying paleosol represents ~3000 years of development on Hauparu tephra (based on Lowe and Hogg, 1995). MSg, Mangaone Subgroup (Jurado-Chichay and Walker, 2000, 2001; Nairn, 2002).

activity since deposition of Rotorua tephra (three events with 2.1 m of displacement in total).

4.2. Sinter development and fault activity

The age of the onset of hydrothermal sinter development in the section on the hill at the Meade site, dated at c. 38.9 ± 1.1 cal ka using radiocarbon, is closely supported by an age (although imprecise) of c. 39.3 ± 2.4 cal. ka on the interbedded Tahuna tephra and by those of the overlying Te Mahoe and Hauparu tephras (c. 36.7 and c. 36.1 cal. ka, respectively; Fig. 8). Sinter formation was discontinuous and stopped before deposition of Kawakawa tephra (c. 25.4 cal. ka; Fig. 9).

In the adjacent trench section, the sinter is younger based on its stratigraphic position in the northeast wall of the trench (Fig. S1). The age of the sinter in the trench is constrained by a maximum of c. 25.4 cal. ka based on the oldest age for Hinuera Formation in the trench, and a minimum of c. 21.8 cal. ka from the overlying Okareka tephra (Fig. 12). Blocks of sinter in between fault planes have not been used to assess its stratigraphic position as these could have been rotated and overturned at the fault plane (Fig. 6).

The timing of this period of sinter development at the Meade site generally mirrors that of the Mangatete sinters on the west strand (Fitzpatrick site) that began forming c. 36 cal. ka (Fig. 1). However, sinter development appears to have ceased entirely at the Meade site by the time Okareka tephra was deposited, while deposition continued between the Rotoma and Taupo eruptive episodes on the west strand near Fitzpatrick trench (Fig. 12).

There are possible connections between the evolution of sinter and fault activity at the Meade site. The fault slip rate analysis (Fig. 11) shows that at the Meade site the Whirinaki Fault decelerated by an order of magnitude at c. 21.8 cal. ka, coincident with the time the sinter deposition ceased. As the fault scarp rapidly grew (> c. 21.8 cal. ka), geothermal activity probably focused around the fault footwall, preferentially depositing sinter at a lower topographic level as the hillside was uplifted, explaining the younger age of the sinter in the trench. Permeability could have been high along this part of the fault through high recurrence in fault rupture (high slip rate) prior to c. 21.8 cal. ka. Deceleration of the slip rate and a subsequent increase in rupture recurrence time (longer time span between events) could have made the fault plane less permeable than other sections of the fault, favouring upflow somewhere else (e.g., in the Fitzpatrick site area, see below). The Meade fault section ruptured a few times after sinter deposition cessation, but less frequently than at the Fitzpatrick site where fault activity (slip rate) increased after the Rotoma eruption (Fig. 11; Canora-Catalán et al. 2008). A period of quiescence in hydrothermal activity in the Mangatete sinters (close to the Fitzpatrick site; Fig. 12) has been associated with relatively low fault activity (Drake et al., 2014).

4.3. Sinter evolution and general landscape development

The stratigraphy in the trench is largely younger than that in the adjacent hill (Figs. 5 and 8). Deposition of the Ohakuri Formation (c. 240 ka), primarily a massive to cross bedded non-welded ignimbrite (which can be locally hardened by cementation; Leonard et al., 2010), formed an extensive subplanar geomorphic surface (hereafter Ohakuri surface) that is currently represented by the highest hills in the landscape (Fig. 2). At c. 39 cal. ka, prior to fluvial incision and the development of a large Whirinaki Fault scarp, geothermal activity at the Meade site was initiated, depositing sinter onto the Ohakuri surface (or most likely onto an eroded Ohakuri surface given the hiatus between Ohakuri Formation and the sinter), possibly onto both the upper and lower topographic levels concurrently as a cascading fault-stepped terrace (as faulting created an escarpment), analogous to those observed in the Orakeikorako geothermal area to the southwest (e.g., Lloyd, 1972; Rowland and Sibson, 2004). With time, both faulting and fluvial incision, along with mass movement, mainly landslides or earthflows of soil and underlying pyroclastic deposits (triggered usually by intense rainstorms, or earthquakes: e.g., Selby, 1967a; Glade, 1998; Crozier, 2005; Basher, 2013), produced a strongly rolling to hilly landscape in poorly consolidated pyroclastic-dominated materials relatively quickly. Landsliding is a common process in hilly geothermal areas (e.g., Newson et al., 2002; Campbell et al., 2004). The downthrown block formed the base of a valley fed by orthogonal shorter valleys that cross the fault scarps on both sides of the small graben (formed along the tilt direction of faulted blocks). The Meade trench is located on one of these side valleys (Fig. 2).

During the period of deposition between the Ohakuri Formation (c. 240 cal. ka) and Kawakawa tephra (c. 25.4 cal. ka), active fluvial, lacustrine, and/or geothermal processes may have prevented the preservation of tephras in the valley, eroding and transporting sediments

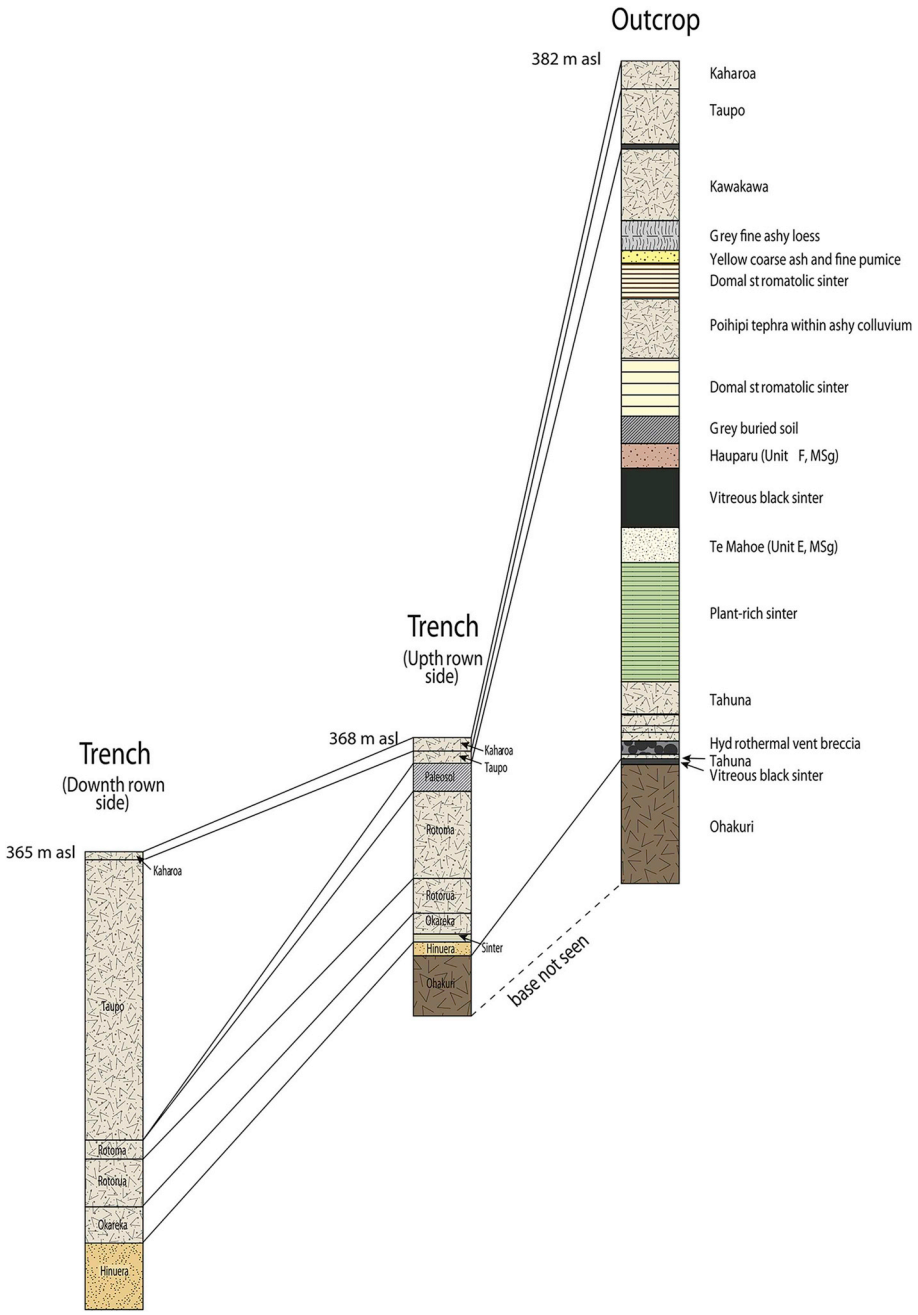

Fig. 9. Correlation of units (Kaharoa and Taupo tephras, a domal stromatolitic sinter, and Ohakuri Formation) in the Meade trench and in the outcrop on the shoulder-slope of the adjacent hill.

away from the lower topographic levels of the landscape, and further deepening the valley despite some aggradation (resulting from infill with mass movement debris) likely occurring as well as incision (e.g., Selby, 1967b). These processes probably accelerated around the time of the last glacial coldest period (LGCP), dated by Barrell et al. (2013) to c. 30–18 cal. ka, which was characterised by strong fluvial and wind erosion (Eden and Hammond, 2003; Lorrey et al., 2012; Newnham et al., 2013; Lorrey and Bostock, 2017) and episodes of landscape instability (McGlone et al., 1984). During the later stages of the LGCP, the Meade site valley was to some extent infilled by the sediments of the Hinuera Formation, in part derived from remobilisation of Kawakawa (equivalent to Oruanui) pyroclastic deposits (Manville and Wilson, 2004; Leonard et al., 2010; Vandergoes et al., 2013). Deep incision of the fluvial drainage along with coeval deposition of Hinuera Formation may have diverted sinter deposition to the lower topographic levels in the valley (perhaps together with fault movement as suggested above). Sinter activity continued for some time after the main fluvial incision (and concomitant mass movement) occurred. By the time of deposition of Okareka tephra at c. 21.8 cal. ka, sinter activity had ceased.

By c. 21.8 cal. ka, the processes of valley erosion seem to have lessened or ceased, enabling the graben and side valleys to act as a basin, capturing the Okareka and younger tephras, with intermittent disruptions by faulting (MH4–MH2) contributing to the deepening of the graben-derived valley and uplifting the side valley. On the adjacent hill, these younger tephras have been eroded with the exception of the Taupo and Kaharoa tephras, which are both < 2 cal. ka in age. The graben was then partly infilled by the unconsolidated Taupo ignimbrite and with subsequent reworked material from the Taupo eruptives (Wilson, 1985; Manville et al., 2009). The infill process reset the landscape (and partially the fault scarp) and subsequent fluvial and

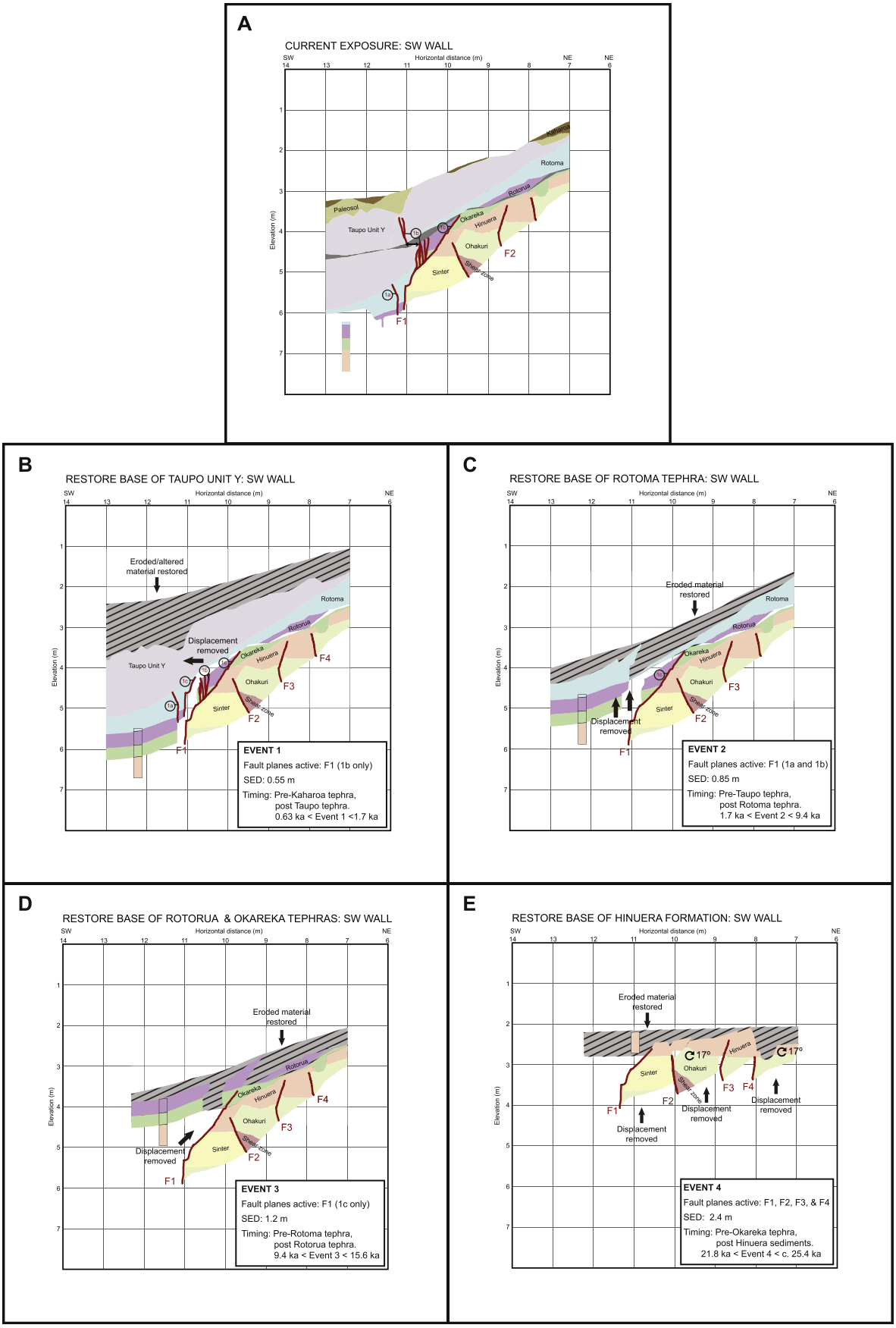

Fig. 10. Restoration of the southwest (SW) wall of the Meade trench. **A** Pre-restoration stratigraphy at present. **B** Restoration of the base of Taupo tephra (unit Y), removing displacement and restoring eroded material from the surface. **C** Restoration of the base of the Rotoma tephra, removing displacement and restoring eroded material from the surface. **D** Restoration of the bases of both the Rotorua and Okareka tephras. **E** Restoration of the base of the Hinuera Formation, removing displacement and sinters, and rotating by 21°. Ages for the tephras (all in cal. ka) are given in Table 2.

Table 3
Fault rupture events from the restoration of the Meade trench and the known ages of the constraining stratigraphic units and mean slip rates.

Fault rupture event	Single event displacement (m)	Constraining units (lower, upper)	Constraining ages (cal. ka)[a]	Mean slip rate (mm/yr)
MH1	0.55 ± 0.2	Taupo tephra, Kaharoa tephra	1.7–0.63	0.508 ± 0.185[b]
MH2	0.85 ± 0.2	Rotoma tephra, Taupo tephra	9.4–1.7	0.110 ± 0.026
MH3	1.2 ± 0.2	Rotorua tephra, Rotoma tephra	15.6–9.4	0.097 ± 0.016
MH4	2.2 ± 0.2	Hinuera Formation[c], Okareka tephra	25.4–21.8	0.629 ± 0.083
Hilltop sinter[d]	8.2 ± 1.5	Kawakawa tephra, Poihipi tephra	28.4–25.4	2.655 ± 0.766

[a] The mean age for each tephra is shown (detailed age ranges are given in Table 2).
[b] Maximum value (incomplete cycle).
[c] The age of the Kawakawa tephra (25.4 cal. ka) is used here as the maximum age for the sediments designated as Hinuera Formation.
[d] The displacement of the hilltop sinter is likely to be cumulative of multiple fault ruptures.

slope processes formed terraces and rolling hills, until further offset by MH1.

In addition to structural controls on the preservation or erosion of deposits, including sinter, regional climatic changes are likely to have played a substantial role in governing the magnitude, frequency, and extent of geomorphic processes occurring at the Meade site, and more widely. Generally cold and windy conditions of the LGCP (comprising New Zealand Climate Events NZce-10, NZce-8, and NZce-6), punctuated by two short interstadials (comprising NZce-9 and NZce-7; Barrell et al., 2013), prevailed in the Rotorua region from c. 30 cal. ka (i.e., from around the time of Poihipi tephra to Kawakawa and Okareka tephras) through to c. 18 cal. ka, just before the deposition of key climatostratigraphic marker bed, the Rerewhakaaitu tephra (c. 17.6 cal. ka; Vucetich and Pullar, 1969; McGlone et al., 1984; Pillans et al., 1993; Newnham et al., 2003). Gradual warming followed, with widespread stabilisation of the landscape occurring after deposition of Rotorua (c. 15.6 cal. ka) and Waiohau (c. 14.0 cal. ka) tephras when forest-dominated vegetation replaced grass-dominated vegetation (Sase et al., 1988; Kondo et al., 1994; Lowe et al., 2012; Barrell et al., 2013). During climatic periods of enhanced erosion, changes in the local hydrology may have induced changes in the spatial distribution of sinters, as the hydrothermal waters flowed to the newly-formed lower geomorphic surfaces; or temporal changes in sinter deposition as changes in the water table level may have precluded or allowed hydrothermal waters to reach the surface.

4.4. Sinter formation and magmatism and volcanic eruptions

Spatial variations on deep magmatic heat sources have been suggested as a possible explanation for rapid evolution of hydrothermal activity in the Ngakuru graben (Kissling et al., 2018). The OVC, located to the northeast of the Meade site (Fig. 1E), has hosted numerous eruptions since its initiation c. 650 ka (Nairn, 2002; Leonard et al., 2010; Cole et al., 2010, 2014, Fig. 13). The latest caldera-forming eruption, which generated the Rotoiti Tephra Formation (Froggatt and Lowe, 1990), occurred at c. 50 cal. ka. This age is uncertain: several different radiometric methods put it between c. 45 and 50 cal. ka (Danišík et al., 2012, 2017; Flude and Storey, 2016), or possibly earlier (Wilson et al., 2007). It was followed almost immediately by the eruption of the (unconsolidated) Earthquake Flat Tephra Formation (Nairn and Kohn, 1973; Froggatt and Lowe, 1990; Nairn, 2002) at c. 45 cal. ka (Danišík et al., 2012). The Earthquake Flat eruption occurred at a series of vents in the Kapenga Volcanic Centre (KVC) only c. 8–10 km northeast of the Meade site (Fig. 13), where much of the hilly landscape is underlain by thick non-welded ignimbrite and minor interbedded fall deposits from the Earthquake Flat eruption (Nairn, 2002). The Rotoiti eruption produced ~80 km^3 of erupted material (volume as dense rock equivalent, DRE), and the Earthquake Flat eruption generated ~7 km^3 (DRE) (Wilson et al., 2007, 2009). A short pulse of intense volcanic activity (generating eruptives of the Mangaone Subgroup: Howorth et al., 1981; Froggatt and Lowe, 1990) occurred from c. 40 to 31 cal. ka

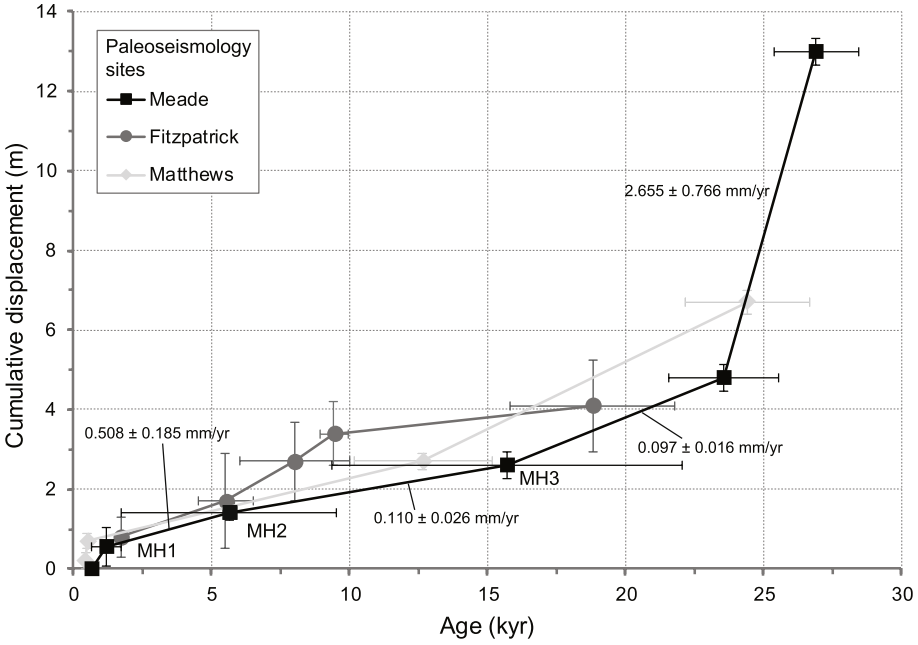

Fig. 11. Age-displacement plot for post-Ohakuri Formation units (Hinuera Formation and Okareka, Rotorua, Rotoma, and Taupo tephras) in the Meade trench compared with values for the Matthews and Fitzpatrick trenches (Canora-Catalán et al. 2008) shown as cumulative offset (metres).

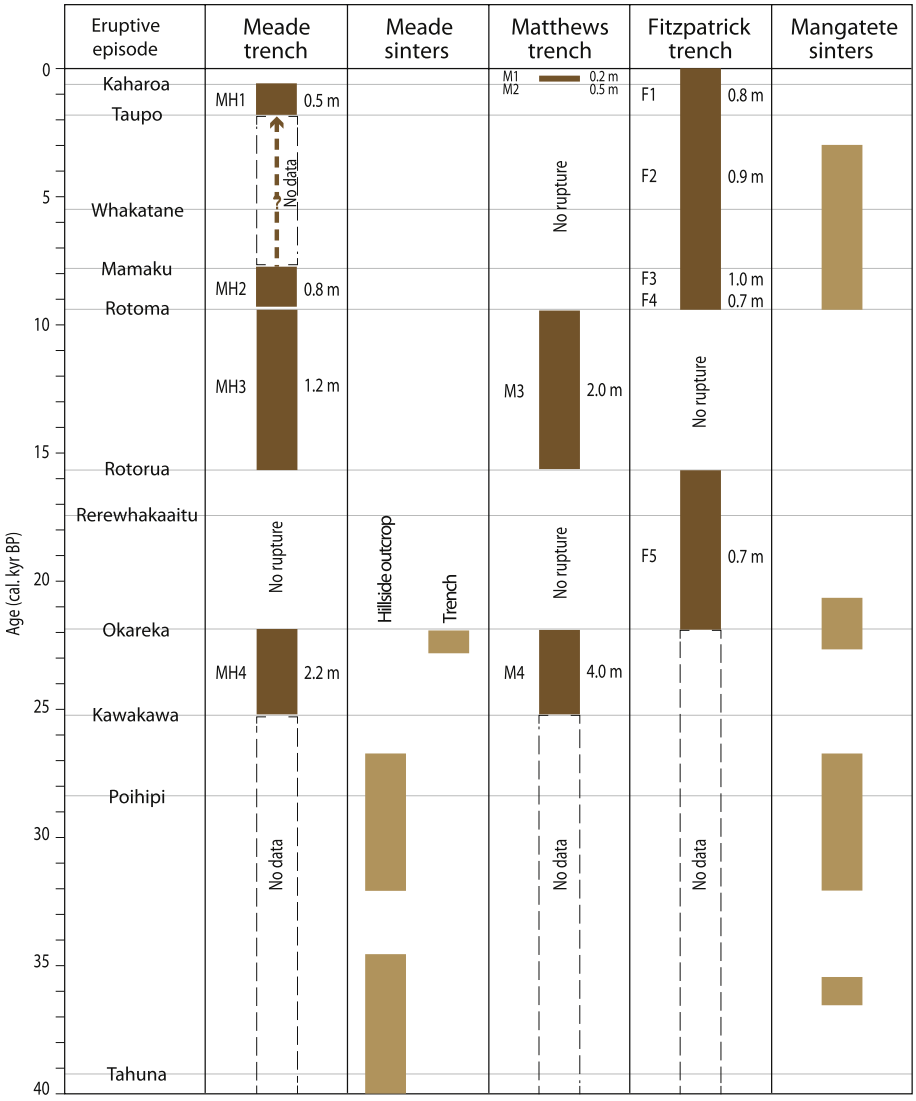

Fig. 12. Summary timeline of fault rupture events and sinter formation from the Meade trench (this study) compared with fault rupture events from the Matthews and Fitzpatrick trenches (Canora-Catalán et al. 2008) and sinter formation at the Mangatete location (Drake et al., 2014). Three tephras listed are additional to those identified in Meade trench and hill section and have ages (95% probability ranges) of 5526 ± 145 cal. yr BP (Whakatane), 7940 ± 257 cal. yr BP (Mamaku), and 17,496 ± 462 cal. yr BP (Rerewhakaaitu) (Lowe et al., 2013). Errors on the ages of the other tephras (eruptive episodes) are given in Table 2.

following the Rotoiti eruption with some of the vents located in the southern part of the OVC (Jurado-Chichay and Walker, 2000, 2001; Smith et al., 2005). Thus, the magmatic sources of volcanism from c. 50 to 31 cal. ka in the southern end of the OVC, and in the northern end of the KVC (Fig. 13), could have provided the heat source for widespread coeval hydrothermal activity at both ~~the~~ Omatokokore (Meade site) and Mangatete (Fitzpatrick site) prior to c. 28 cal. ka. At the Meade site, hydrothermal vent breccias intercalated with sinter and the Tahuna tephra indicate that vigorous surface hydrothermal activity was associated with the initiation of geothermal activity and reorganising of fluid pathways in this region at c. 40 cal. ka. The stratigraphy interpreted from drillhole TH1 (Fig. 1B) that encountered ~40 m of hydrothermal vent breccia (Alder and Sharp, 1988) suggests that the hydrothermal vent breccia (Fig. 8) in the hillside outcrop may be the distal edge of a more widespread hydrothermal eruption deposit. Hydrothermal eruptions at the initiation of geothermal activity are observed elsewhere and are analogous to widespread hydrothermal eruptions in the Waimangu Valley associated with hydrological changes in the Rotomahana-Waimangu hydrothermal system after the 10 June 1886 Tarawera eruption (Nairn, 1979; Simmons et al., 1993) (although we recognise that hydrothermal eruptions can occur at almost any stage in the evolution of a geothermal system).

In the last c. 25 cal. kyr, most eruptions have been sourced from two linear vent zones, Haroharo and Tarawera, within OVC (Fig. 13; Nairn, 2002; Smith et al., 2005; Cole et al., 2010, 2014). Other vents occur on the periphery of these zones: Okareka and Rotoma embayments lie on the Haroharo Linear Vent Zone, whereas Puhipuhi Embayment and Lake Rotomahana Basin/Crater lie on the Tarawera Linear Vent Zone (Fig. 13). Drake et al. (2014) suggested that there is a cluster of sinter dates at Mangatete that coincide with the Okareka eruption, which was sourced from the Tarawera lineament (Nairn, 1992, 2002), about 20 km away from Mangatete sinters. However, without further subsurface investigations in the area we cannot preclude the presence of more local magmatism in this period.

4.5. Sinter evolution at the Meade site

We have proposed several potential controls on sinter evolution including tectonic, volcanic (magmatic), or climatic (geomorphic) processes. With the information available it is difficult to select one as the major driver. Although sinter formation was demonstrably discontinuous at the Omatokokore (and Mangatete) site, hydrothermal

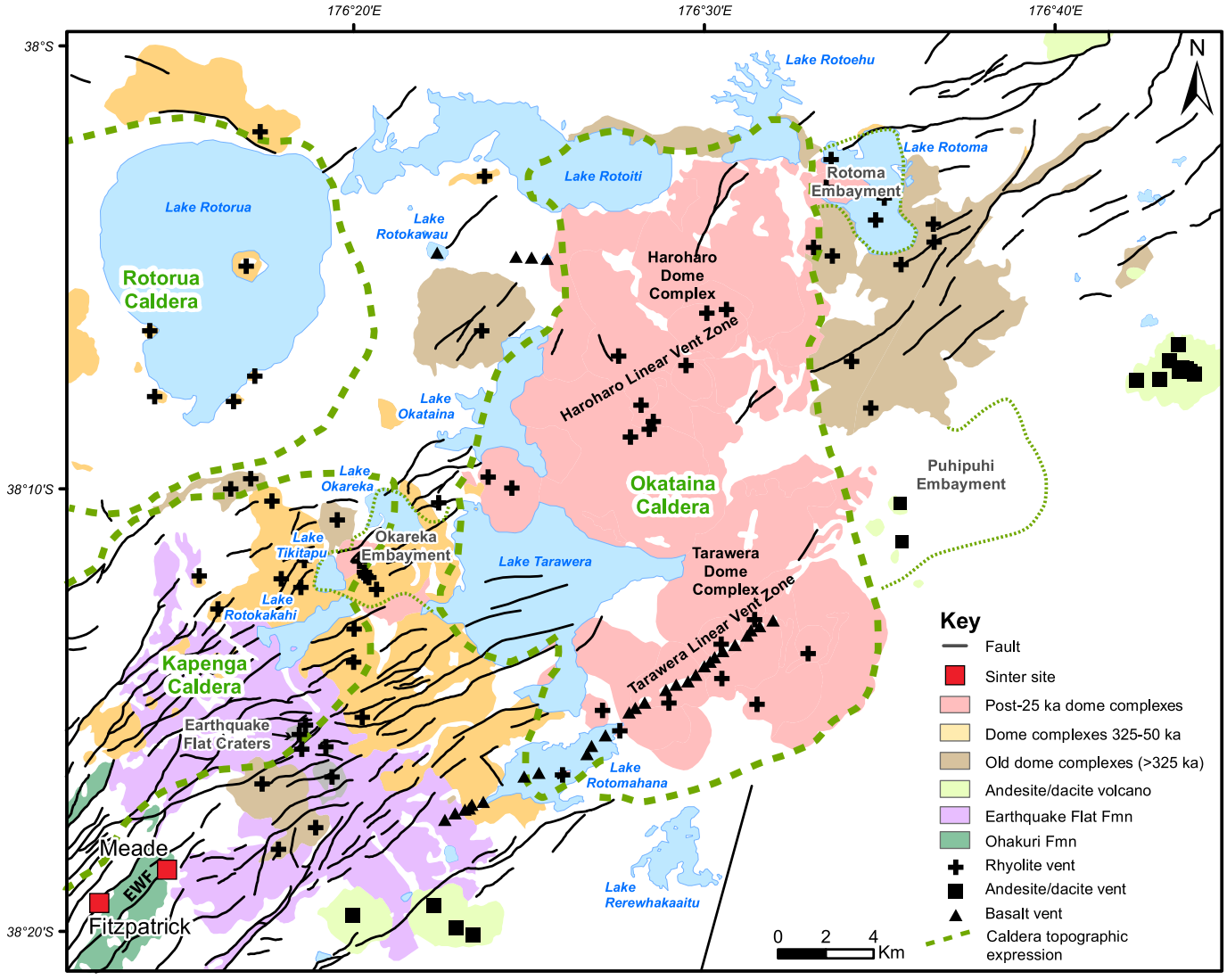

Fig. 13. Simplified volcanic geology of the Okataina Volcanic Centre including lava dome complexes (all of which were deposited in association with multiple pyroclastic eruptives: Nairn, 2002) and their general ages, and locations of the main faults. The northern part of the adjacent Kapenga Volcanic Centre, which hosts the Ngakuru Graben and the Meade study site just to the southwest (Fig. 1E), is also indicated. EWF, East Whirinaki Fault. After Nairn (2002), Leonard et al. (2010), and Cole et al. (2014).

activity in the area may have been continuous but with some interruptions. Findings from our study can only be related to hydrothermal activity in the local area and, although activity may have ceased at this specific outcrop, changes in fluid pathways may have resulted in sinter deposition moving to a location beyond the study area. Hydrothermal activity may also still be occurring at depth, but with no current surface manifestation. In light of the multiple controlling factors exposed here, it is clear that the further understanding of sinter dynamics (changes in location and causes) requires the construction of high-resolution maps of sinter distribution in the region, including the areas where the fossil sinters are covered by Holocene tephras, which may comprise the largest extent.

For the sinters along the Whirinaki Fault, Omatokokore (Meade site), and Mangatete (Fitzpatrick site) localities, we tentatively propose that extensive hydrothermal activity may have been present in association with the Rotoiti caldera-forming eruption and with the subsequent intense and complex magmatic activity through to c. 31 cal. ka (Smith et al., 2005; Charlier and Wilson, 2010). The topography of the landscape along the fault may have still been controlled by extensive subhorizontal constructional surfaces (e.g., eroded Ohakuri surface). More recently control came from the deposition of the non-welded pyroclastics underlying the Earthquake Flat surface in the area southwest of OVC and in the northern KVC (Leonard et al., 2010, Fig. 13), which also favoured widespread sinter deposition. Changes in topography, mainly post c. 25.4 cal. ka, including development of deep valleys (climatic and tectonic controlled), diverted surface hot spring flows and localised them in topographic lows. Sinter formation at the surface could even temporarily disappear depending on water table levels. With waning of the large-scale heat source, and stabilisation of the landscape soon after the LGCP during the Last Glacial-Interglacial Transition (LGIT) (e.g., Newnham et al., 2003; Barrell et al., 2013), reactivation of sinter deposition can be associated with the appearance of local heat sources or to variation on fault activity rate. For example, diversion of flow to lower areas or changes in water table once the landscape is stabilised, may explain why, during the Okareka eruption, sinter activity was reactivated at the Mangatete site at the surface (Drake et al., 2014), but not at Omatokokore (despite the latter being 4 km closer to Okareka eruption vents and heat source in the Tarawera Linear Vent Zone). Higher slip rates on the Meade site prior to c. 21 cal. ka may have strongly influenced topography at that site (Fig. 2A) and thus loss of surface flow of hydrothermal waters post-21 cal. ka, whereas higher slip rates at the Fitzpatrick site after c. 10 cal. ka may

explain the presence of the most recent sinters at Mangatete as a consequence of enhanced crustal permeability (and enhanced fluid upflow). In any event, further evaluation of these earlier trench and sinter study sites using high-resolution topographic maps derived from LiDAR, together with shallow trenching, coring or drilling, near-surface geophysics (and so on), would be appropriate to help link the faulting and sinter development with landscape evolution.

In summary, our study, in combination with the results from prior studies, suggests that the Whirinaki Fault has been an important location for shallow hydrothermal flow at least for the last c. 40 cal. kyr. Surficial sinter activity suggests that shallow hydrothermal activity that could be exploited for geothermal energy lasts between 1000 and 7000, or more, years. However, we do not know whether the activity still persists at depth during times of quiescence in surface deposition of sinters, or whether the whole system switches on and off. Better understanding of past geothermal activity, and the factors that control its evolution (e.g., periods of quiescence, or lack of surface expression), is fundamental in evaluating the viability of geothermal energy exploitation.

5. Conclusions

(1) By combining stratigraphy with mineralogical and geochemical fingerprinting, five late Quaternary tephras of known age were identified at the Meade trench, namely the Kaharoa, Taupo, Rotoma, Rotorua, and Okareka tephras, together with the Ohakuri Formation (a non-welded ignimbrite). In an outcrop on the upper part (shoulder-slope) of an adjacent hill, the Kaharoa, Taupo, Kawakawa, Poihipi, Hauparu, Te Mahoe, and Tahuna tephras, and the Ohakuri Formation, were also identified. The younger tephras especially have well-established ages (Table 2). These ages, together with the newly reported radiocarbon age on plant microfossil material (c. 38.9 cal. ka) entrained in sinter interbedded with Tahuna tephra (c. 39.3 cal. ka) on the hill, were able to be transferred using tephrochronology to the Meade sequences, thereby providing a chronostratigraphic framework to evaluate and date the history of events and deposition inferred at the site including faulting and hydrothermal activity.

(2) A history of displacement was determined in the trench, with five discernible fault rupture events (MH5 to MH1). MH5 is the oldest and most poorly constrained event, occurring after emplacement of Ohakuri Formation (c. 240 ka) and prior to deposition of the Hinuera Formation (c. 25.4 cal. ka). MH4 occurred between deposition of the Hinuera Formation (c. 25.4 cal. ka) and Okareka tephra (c. 21.8 cal. ka). MH3 occurred between the deposition of Rotorua tephra (c. 15.6 cal. ka) and Rotoma tephra (c. 9.4 cal. ka). MH2 occurred between the deposition of Rotoma tephra (c. 9.4 cal. ka) and Taupo tephra (c. 1.7 cal. ka). MH1 is the most recent, occurring after the deposition of Taupo tephra (c. 1.7 cal. ka).

(3) Based on the tephrochronology and the new radiocarbon date, the Omatokokore sinters at the Meade site were deposited between c. 39 cal. ka and c. 21.8 cal. ka. This hydrothermal activity is similar in timing to the early activity – generating the Mangatete sinters – recorded on the west strand of the Whirinaki Fault at the Fitzpatrick site dating from c. 36 cal. ka to c. 21.6 cal. ka. The cessation of activity at the Meade site (c. 21.8 cal. ka) is not known to have been matched at the Fitzpatrick site, where active sinter deposition continued through the late Pleistocene and well into the Holocene. A combination of factors that may explain the different evolution of the surficial sinter activity at both sites is proposed here. Extensive sinter activity at both sites prior to c. 31 cal. ka may be explained by the presence of a large magmatic heat source at the southern end of the Okataina Volcanic Centre (c. 50 to 31 cal. ka), and in the northern end of the adjacent Kapenga Volcanic Centre (c. 45 cal. ka), and a subhorizontal topography related to emplacement of (non-welded) ignimbrites and associated deposits that reset the landscape. During this period, siliceous sinters were being actively deposited at both sites.

(4) Climatic conditions associated with the last glacial coldest period c. 30–18 cal. ka, and general warming and moistening afterwards during the LGIT (Barrell et al., 2013), together with the unconsolidated nature of the pyrocastic eruptives, dictated relatively fast rates of fluvial incision and mass movement events that together helped shape the modern landscape. Fault activity, resulting in the localisation of subsidence, strongly affected the landscape as well, creating topographic low points locally to which surface waters were diverted, and possible changes in water table levels. Once the larger heat source(s) had waned, and the landscape stabilised, deposition of sinters at the surface may be controlled by magmatic heat sources associated with less voluminous eruptions. Previous studies have linked the Okareka eruption (c. 21.8 cal. ka) with the onset of deposition of the Mangatete sinter (Drake et al., 2014), but only if the topographic conditions were favourable (this caveat may explain why no sinter activity occurred at the Omatokokore sinters in association with that eruption). Also, temporal variation of fault activity can be held responsible for enhancement of crustal permeability in the Mangatete sinters area with subsequent sinter deposition occurring after c. 10 cal. ka. During this latest period (post-10 cal. ka), sinters did not form at the surface at the Omatokokore site, coincident with lower levels of fault activity or because of an unfavourable topographic situation, or both.

(5) This study is the first to use tephrochronology to constrain ages for both fault rupture and hydrothermal activity at a single location, reinforcing its usefulness as a chronostratigraphic tool in complex and active geological settings such as the central TVZ. The findings improve understanding of the complex rupture behaviour of the Whirinaki Fault and provide evidence for relationships between tectonic, climatic, and hydrothermal activity. This study contributes to a better understanding of the evolution and life span of important energy resources associated with geothermal systems. The data collected and evaluated from the trench restoration may also be useful for seismic hazard assessment modelling because the Whirinaki Fault is one of the major faults in the Taupo Rift within the central TVZ.

Acknowledgements

We thank the Meade family for access to the field site and John and Catherine Ford for accommodation, Renat Radosinsky and Janine Ryburn (University of Waikato) for help with sample preparation, Dean Sandwell and Annette Rogers (University of Waikato) for vibrocoring, and Ian Schipper (Victoria University of Wellington) for providing setup and guidance for EPMA. Ian Nairn is especially thanked for his assistance in the field early in the study. Helpful and positive comments by reviewers Pat Browne and Maria Ortuño were greatly appreciated and enabled us to improve the paper considerably. The project was funded by MBIE SSIF funds and the University of Waikato. RCL acknowledges support provided by the Broad Memorial Fund and University of Waikato Summer Research and Masterate Research scholarships. The paper is an output of a Strategic Investment Fund (Research) grant F719 of the University of Waikato and was completed in conjunction with support from the Earthquake Commission of New Zealand for another project (EQC grant 15/U713). It is also an output of the EXTRAS project "EXTending TephRAS as a global geoscientific research tool stratigraphically, spatially, analytically, and temporally" led by the International focus group on tephrochronology and volcanism (INTAV) of the Stratigraphy and Chronology Commission (SACCOM) of the International Union for Quaternary Research (INQUA) for 2015–2019. We especially thank the editor-in-chief of *Quaternary International*, Prof Thijs van Kolfschoten, for inviting us to contribute this paper to the special 500th volume of the journal.

Appendix A. Supplementary data

Supplementary data to this article can be found online at https://doi.org/10.1016/j.quaint.2019.02.031.

References

Adams, C.A., Auld, A.M.C., Gluyas, J.G., Hogg, S., 2015. Geothermal energy – the global opportunity. Proc. Inst. Mech. Eng., Part A: Journal and Energy 229 (7), 747.

Alder, G.A., Sharp, B.M., 1988. Report on Geology, Geochemistry and Geophysics, PL 311941 (Thomsons), Central North Island. Ministry of Economic Development New Zealand Unpublished Mineral Report MR671.

Barrell, D.J.A., Almond, P.C., Vandergoes, M.J., Lowe, D.J., Newnham, R.M., NZ-INTIMATE members, 2013. A composite pollen-based stratotype for inter-regional evaluation of climatic events in New Zealand over the past 30,000 years (NZ-INTIMATE project). Quat. Sci. Rev. 74, 4–20.

Basher, L.R., 2013. Erosion processes and their control in New Zealand. In: Dymond, J.R. (Ed.), Ecosystem Services in New Zealand – Conditions and Trends. Manaaki Whenua Press, Lincoln, New Zealand, pp. 363–374.

Beanland, S., Berryman, K.R., Blick, G.H., 1989. Geological investigations of the 1987 Edgecumbe earthquake, New Zealand. N. Z. J. Geol. Geophys. 32, 73–91.

Berryman, K., Villamor, P., Nairn, I., van Dissen, R., Begg, J., Lee, J., 2008. Late Pleistocene surface rupture history of the Paeroa fFault, Taupo Rift, New Zealand. N. Z. J. Geol. Geophys. 51, 135–158.

BOPLASS, 2013. accessed on 25/10/2018. http://www.boplass.co.nz/.

Brathwaite, R.L., 2003. Geological and mineralogical characterization of zeolites in lacustrine tuffs, Ngakuru, Taupo Volcanic Zone, New Zealand. Clay Clay Miner. 51, 589–598.

Bronk Ramsey, C., 2009. Bayesian analysis of radiocarbon dates. Radiocarbon 51, 337–360.

Bryan, C.J., Sherburn, S., Bibby, H.M., Bannister, S.C., Hurst, A.W., 1999. Shallow seismicity of the central Taupo Volcanic Zone, New Zealand: its distribution and nature. N. Z. J. Geol. Geophys. 42 (4), 533–542.

Campbell, K.A., Sannazzaro, K., Rodgers, K.A., Herdianita, N.R., Browne, P.R.L., 2001. Sedimentary facies and mineralogy of the late Pleistocene Umukuri silica sinter, Taupo Volcanic Zone, New Zealand. J. Sediment. Res. 71, 727–746.

Campbell, K.A., Buddle, T.F., Browne, P.R.L., 2004. Late Pleistocene siliceous sinter associated with fluvial, lacustrine, volcaniclastic and landslide deposits at Tahunaatara, Taupo Volcanic Zone, New Zealand. Trans. R. Soc. Edinb. Earth Sci. 94, 485–501.

Canora-Catalán, C., Villamor, P., Berryman, K., Martínez-Díaz, J.J., Raen, T., 2008. Rupture history of the Whirinaki Fault, an active normal fault in the Taupo Rift, New Zealand. N. Z. J. Geol. Geophys. 51, 277–293. https://doi.org/10.1080/00288300809509866.

Chambefort, I., Bignall, G., 2016. Taupo Volcanic Zone Geothermal Systems, New Zealand: Exploration, Science and Development. Special Issue 59, Part B, Geothermics.

Charlier, B.L.A., Wilson, C.J.N., 2010. Chronology and evolution of caldera-forming and post-caldera magma systems at Okataina Volcano, New Zealand, from zircon U–Th model-age spectra. J. Petrol. 51, 1121–1141.

Cole, J.W., Spinks, K.D., Deering, C.D., Nairn, I.A., Leonard, G.S., 2010. Volcanic and structural evolution of the Okataina Volcanic Centre; dominantly silicic volcanism associated with the Taupo Rift, New Zealand. J. Volcanol. Geoth. Res. 190, 123–135.

Cole, J.W., Deering, C.D., Nairn Burt, R.M., Sewell, S., Shane, P.A.R., Matthews, N.E., 2014. Okataina Volcanic Centre, Taupo Volcanic Zone, New Zealand: a review of volcanism and synchronous pluton development in an active, dominantly silicic caldera system. Earth Sci. Rev. 128, 1–17.

Crozier, M.J., 2005. Multiple-occurrence regional landslide events in New Zealand: hazard management issues. Landslides 2, 247–256.

Danišík, M., Shane, P.A.R., Schmitt, A.K., Hogg, A.G., Santos, G.M., Storm, S., Evans, N.J., Fifield, L.K., Lindsay, J.M., 2012. Re-anchoring the late Pleistocene tephrochronology of New Zealand based on concordant radiocarbon ages and combined $^{238}U/^{230}Th$ disequilibrium and (U-Th)/He zircon ages. Earth Planet. Sci. Lett. 349–350, 240–250.

Danišík, M., Schmitt, A.K., Lovera, O.M., Dunkl, I., Evans, N.J., 2017. Application of the combined U-Th-disequilibrium/U-Pb and (U-Th)/He zircon dating to tephrochronology. Quat. Geochronol. 40, 23–32.

Drake, B.D., Campbell, K.A., Rowland, J.V., Guido, D.M., Browne, P.R., Rae, A., 2014. Evolution of a dynamic paleo-hydrothermal system at Mangatete, Taupo volcanic zone. J. Volcanol. Geoth. Res. 282, 19–35. https://doi.org/10.1016/j.jvolgeores.2014.06.010.

Dunbar, N.W., Iverson, N.A., Van Eaton, A.R., Sigl, M., Alloway, B.V., Kurbatov, A.V., Mastin, L.G., McConnell, J.R., Wilson, C.J.N., 2017. New Zealand supereruption provides time marker for the Last Glacial Maximum in Antarctica. Sci. Rep. 7, 12238.

Eden, D.N., Hammond, A.P., 2003. Dust accumulation in the New Zealand region since the last glacial maximum. Quat. Sci. Rev. 22, 2037–2052.

Flude, S., Storey, M., 2016. $^{40}Ar/^{39}Ar$ age of the Rotoiti Breccia and Rotoehu Ash, Okataina Volcanic Complex, New Zealand, and identification of heterogeneously distributed excess ^{40}Ar in supercooled crystals. Quat. Geochronol. 33, 13–23.

Froggatt, P.C., Gosson, G.J., 1982. Techniques for the Preparation of Tephra Samples for Mineral and Chemical Analysis and Radiometric Dating, vol. 23. Geology Department, Victoria University of Wellington Publication, pp. 1–12.

Froggatt, P.C., Lowe, D.J., 1990. A review of late Quaternary silicic and some other tephra formations from New Zealand: their stratigraphy, nomenclature, distribution, volume, and age. N. Z. J. Geol. Geophys. 33, 89–109. https://doi.org/10.1080/00288306.1990.10427576.

Glade, T., 1998. Establishing the frequency and magnitude of landslide-triggering rainstorm events in New Zealand. Environ. Geol. 35, 160–174.

Gravley, D.M., Wilson, C.J.N., Rosenberg, M.D., Leonard, G.S., 2006. The nature and age of Ohakuri Formation and Ohakuri Group rocks in surface exposures and geothermal drillhole sequences in the central Taupo Volcanic Zone, New Zealand. N. Z. J. Geol. Geophys. 49, 305–308.

Gravley, D.M., Wilson, C.J.N., Leonard, G.S., Cole, J.W., 2007. Double trouble: paired ignimbrite eruptions and collateral subsidence in the Taupo Volcanic Zone, New Zealand. Geol. Soc. Am. Bull. 119, 18–30.

Hall, M., Hayward, C., 2014. Preparation of micro-and crypto-tephras for quantitative microbeam analysis. Geol. Soc. Spec. Publ. 398, 21–28. https://doi.org/10.1144/SP398.5.

Heise, W., Bibby, H.M., Grant, C.T., Bannister, S.C., Ogawa, Y., Takakura, S., Uchida, T., 2007. Melt distribution beneath a young continental rift; the Taupo Volcanic Zone, New Zealand. Geophys. Res. Lett. 34, L14313. https://doi.org/10.1029/2007GL029629.

Heise, W., Caldwell, T.G., Bibby, H.M., Bennie, S.L., 2010. Three-dimensional electrical resistivity image of magma beneath an active continental rift, Taupo Volcanic Zone, New Zealand. Geophys. Res. Lett. 37, L10301. https://doi.org/10.1029/2010GL043110.

Hogg, A.G., Higham, T.F.G., Lowe, D.J., Palmer, J., Reimer, P., Newnham, R.M., 2003. A wiggle-match date for Polynesian settlement of New Zealand. Antiquity 77, 116–125.

Hogg, A.G., Lowe, D.J., Palmer, J.G., Boswijk, G., Bronk Ramsey, C.J., 2012. Revised calendar date for the Taupo eruption derived by ^{14}C wiggle-matching using a New Zealand kauri ^{14}C calibration data set. Holocene 22, 439–449.

Hogg, A., Hua, Q., Blackwell, P.G., Niu, M., Buck, C.E., Guilderson, T.P., Heaton, T.J., Palmer, J.G., Reimer, P.J., Reimer, R.W., Turney, C.S.M., Zimmerman, S.R.H., 2013. SHCal13 Southern Hemisphere calibration, 0–50,000 years cal. BP. Radiocarbon 55, 1–15.

Holland, G.R., 2000. The Whirinaki Sinter, Taupo Volcanic Zone [Unpublished MSc Thesis]. University of Auckland, Auckland.

Howorth, R., Froggatt, P.C., Vucetich, C.G., Collen, J.D., 1981. Publication of Geology Department Victoria University of WellingtonEditorial. In: Proceedings of a Tephra Workshop, 30 June-1 July 1980, Victoria University of Wellington, vol. 20. pp. 1–4.

Hurst, T., Bannister, S., Robinson, R., Scott, B., 2008. Characteristics of three recent earthquake sequences in the Taupo Volcanic Zone, New Zealand. Tectonophysics 452 (1–4), 17–28.

Janoušek, V., Farrow, C.M., Erban, V., 2006. Interpretation of whole-rock geochemical data in igneous geochemistry: introducing Geochemical Data Toolkit (GCDkit). J. Petrol. 47, 1255–1259. https://doi.org/10.1093/petrology/egl013.

Janoušek, V., Farrow, C.M., Erban, V., Trubač, J., 2011. Brand new geochemical data toolkit (GCDkit 3.0) – is it worth upgrading and browsing documentation? (Yes!). Geol výzk Mor Slez. 18, 26–30.

Jarosewich, E., Nelen, J.A., Norberg, J.A., 1980. Reference samples for electron microprobe analysis. Geostand. Newsl. 4, 43–47. https://doi.org/10.1111/j.1751-908X.1980.tb00273.x.

Jochum, K.P., Stoll, B., Herwig, K., Willbold, M., Hofmann, A.W., Amini, M., Aarburg, S., Abouchami, W., Hellebrand, E., Mocek, B., Raczek, I., Stracke, A., Alard, O., Bouman, C., Becker, S., Dücking, M., Brätz, H., Klemd, R., de Bruin, D., Canil, D., Cornell, D., de Hoog, C., Dalpé, C., Danyushevsky, L., Eisenhauer, A., Gao, Y., Snow, J.E., Groschopf, N., Günther, D., Latkoczy, C., Guillong, M., Hauri, E.H., Höfer, H.E., Lahaye, Y., Horz, K., Jacob, D.E., Kasemann, S.A., Kent, A.J.R., Ludwig, T., Zack, T., Mason, P.R.D., Meixner, A., Rosner, M., Misawa, K., Nash, B.P., Pfänder, J., Premo, W.R., Sun, W.D., Tiepolo, M., Vannucci, R., Vennemann, T., Wayne, D., Woodhead, J.D., 2006. MPI-DING reference glasses for in situ microanalysis: new reference values for element concentrations and isotope ratios. Geochem. Geophys. Geosyst. 7, 1–44. https://doi.org/10.1029/2005GC001060.

Jones, B., Renaut, R.W., Torfason, H., Owen, R.B., 2007. The geological history of Geysir, Iceland: a tephrochronological approach to the dating of sinter. J. Geol. Soc. 164, 1241–1252.

Jurado-Chichay, Z., Walker, G.P.L., 2000. Stratigraphy and dispersal of the Mangaone Subgroup pyroclastic deposits, Okataina Volcanic Centre, New Zealand. J. Volcanol. Geoth. Res. 104, 319–389.

Jurado-Chichay, Z., Walker, G.P.L., 2001. The intensity and magnitude of the Mangaone Subgroup plinian eruptions from Okataina Volcanic Centre, New Zealand. J. Volcanol. Geoth. Res. 111, 219–237.

Kissling, W.M., Villamor, Ellis, SM., Rae, A.J., 2018. Modelling of hydrothermal fluid flow and structural architecture in an extensional basin, Ngakuru Graben, Taupo Rift, New Zealand. J. Volcanol. Geoth. Res. 357, 134–151.

Kondo, R., Childs, C., Atkinson, I., 1994. Opal Phytoliths of New Zealand. Manaaki Whenua Press, Lincoln, New Zealand.

Kuehn, S.C., Froese, D.G., Shane, P.A.R., 2011. The INTAV intercomparison of electron-beam microanalysis of glass by tephrochronology laboratories: results and recommendations. Quat. Int. 246, 19–47. https://doi.org/10.1016/j.quaint.2011.08.022.

Lane, C.S., Lowe, D.J., Blockley, S.P.E., Suzuki, T., Smith, V.C., 2017. Advancing tephrochronology as a global dating tool: applications in volcanology, archaeology, and palaeoclimatic research. Quat. Geochronol. 40, 1–7.

Langridge, R.M., Ries, W.F., Farrier, T., Barth, N.C., Khajavi, N., De Pascale, G.P., 2014. Developing sub 5-m LiDAR DEMs for forested sections of the alpine and hope faults, South Island, New Zealand: implications for structural interpretations. J. Struct. Geol. 64, 53–66.

Leonard, G.S., Begg, J.G., Wilson, C.J.N., 2010. In: Geology of the Rotorua Area: Scale 1: 250,000. Institute of Geological and Nuclear Sciences 1: 250,000 Geological Map, vol. 5 Lower Hutt: GNS Science, New Zealand.

Lian, O.B., Shane, P.A.R., 2000. Optical dating of paleosols bracketing the widespread Rotoehu tephra, North Island, New Zealand. Quat. Sci. Rev. 19, 1649–1662.

Lloyd, E.F., 1972. Geology and hot springs of Orakeikorako. N. Z. Geol. Surv. Bull. 85, 164.

Loame, R.C., 2016. Using a Tephrostratigraphic Framework to Determine the Past 40,000 Yrs of Rupture and Paleohydrothermal Activity on the East Strand of the Whirinaki Fault, Ngakuru Graben, Central Taupo Volcanic Zone. Unpublished MSc thesis, University of Waikato, Hamilton, New Zealand.

Lorrey, A.M., Bostock, H., 2017. The climate of New Zealand thought the Quaternary. In:

Shulmeister, J. (Ed.), Landscape and Quaternary Environmental Change in New Zealand. Springer/Atlantis Press, pp. 67–139.
Lorrey, A.M., Vandergoes, M., Almond, P., Renwick, J., Stephens T, Bostock, H., Mackintosh, A., Newnham, R., Williams, P.W., Ackerley, D., Neil, H., Fowler, A.M., 2012. Palaeocirculation across New Zealand during the last glacial maximum at ~21 ka. Quat. Sci. Rev. 36, 189–213.
Lowe, D.J., 2011. Tephrochronology and its application: a review. Quat. Geochronol. 6, 107–153. https://doi.org/10.1016/j.quageo.2010.08.003.
Lowe, D.J., Alloway, B.V., 2015. Tephrochronology. In: Rink, W.J., Thompson, J.W. (Eds.), Encyclopedia of Scientific Dating Methods. Springer, Dordrecht, pp. 783–799.
Lowe, D.J., Hogg, A.G., 1995. Age of the Rotoehu Ash. N. Z. J. Geol. Geophys. 38, 399–402.
Lowe, D.J., Palmer, D.J., 2005. Andisols of New Zealand and Australia. J. Int. Field Sci. 2, 39–65.
Lowe, D.J., McFadgen, B.G., Higham, T.F.G., Hogg, A.G., Froggatt, P.C., Nairn, I.A., 1998. Radiocarbon age of the Kaharoa Tephra, a key marker for late-Holocene stratigraphy and archaeology in New Zealand. Holocene 8, 487–495.
Lowe, D.J., Shane, P.A., Alloway, B.V., Newnham, R.M., 2008. Fingerprints and age models for widespread New Zealand tephra marker beds erupted since 30,000 years ago: a framework for NZ-INTIMATE. Quat. Sci. Rev. 27, 95–126.
Lowe, D.J., Lanigan, K.M., Palmer, D.J., 2012. Where geology meets pedology: late Quaternary tephras, loess, and paleosols in the Mamaku Plateau and Lake Rerewhakaaitu areas. Geosci. Soc. New Zeal. Misc. Pub. 134B 2.1 – 2.45.
Lowe, D.J., Blaauw, M., Hogg, A.G., Newnham, R.M., 2013. Ages of 24 widespread tephras erupted since 30,000 years ago in New Zealand, with re-evaluation of the timing and palaeoclimatic implications of the late glacial cool episode recorded at Kaipo bog. Quat. Sci. Rev. 74, 170–194. https://doi.org/10.1016/j.quascirev.2012.11.022.
Lowe, D.J., Pearce, N.J.G., Jorgensen, M.A., Kuehn, S.C., Tryon, C.A., Hayward, C.L., 2017. Correlating tephras and cryptotephras using glass compositional analyses and numerical and statistical methods: review and evaluation. Quat. Sci. Rev. 175, 1–44.
Manville, V., Wilson, C.J.N., 2004. The 26.5 ka Oruanui eruption, New Zealand: a review of the roles of volcanism and climate in the post-eruptive sedimentary response. N. Z. J. Geol. Geophys. 47, 525–547.
Manville, V., Swegschneider, B., Newton, E., White, J.D.L., Houghton, B.F., Wilson, C.J.N., 2009. Environmental impact of the 1.8 ka Taupo eruption, New Zealand: landscape responses to a large-scale explosive rhyolite eruption. Sediment. Geol. 220, 318–336.
McCalpin, J.P., 2009. Field techniques in paleoseismology—terrestrial environments. Int. Geophys. 95, 29–118. https://doi.org/10.1016/S0074-6142(09)95002-1.
McGlone, M.S., Howorth, R., Pullar, W.A., 1984. Late Pleistocene stratigraphy, vegetation and climate of the Bay of Plenty and Gisborne regions, New Zealand. N. Z. J. Geol. Geophys. 27, 327–350.
Molloy, C., Shane, P., Augustinus, P.C., 2009. Eruption recurrence rates in a basaltic volcanic field based on tephra layers in maar sediments: implications for hazards in the Auckland volcanic field. Geol. Soc. Am. Bull. 121, 1666–1677.
Mouslopoulou, V., Nicol, A., Little, T.A., Walsh, J.J., 2007. Terminations of large strike-slip faults: an alternative model from New Zealand. Geol. Soc. Spec. Publ. 290, 387–415.
Nairn, I.A., 1979. Rotomahana – Waimangu eruption, 1886: base surge and basalt magma. N. Z. J. Geol. Geophys. 22, 363–378.
Nairn, I.A., 1992. The Te Rere and Okareka eruptive episodes — Okataina Volcanic Centre, Taupo volcanic zone, New Zealand. N. Z. J. Geol. Geophys. 35, 93–108.
Nairn, I.A., 2002. In: Geology of the Okataina Volcanic Centre, Scale 1:50,000. Institute of Geological and Nuclear Sciences Geological Map 25 Lower Hutt: GNS Science, New Zealand.
Nairn, I.A., Kohn, B.P., 1973. Relation of the Earthquake Flat Breccia to the Rotoiti Breccia, central North Island, New Zealand. N. Z. J. Geol. Geophys. 16 (2), 269–279.
Newnham, R.M., Eden, D.N., Lowe, D.J., Hendy, C.H., 2003. Rerewhakaaitu Tephra, a land-sea marker for the Last Termination in New Zealand, with implications for global climate change. Quat. Sci. Rev. 22, 289–308.
Newnham, R.M., McGlone, M.S., Moar, N., Wilmshurst, J.M., Vandergoes, M.J., 2013. The vegetation cover of New Zealand at the Last Glacial Maximum. Quat. Sci. Rev. 74, 202–214.
Newson, A.M., Pebble, W.M., Browne, P.R.L., 2002. Landsliding on the Paeroa Fault at Te Kopia. In: Soengkono, S., Browne, P.R.L. (Eds.), Proceedings of the 24th New Zealand Geothermal Workshop, Auckland, pp. 61–65.
Nicol, A., Walsh, J., Berryman, K., Villamor, P., 2006. Interdependence of fault displacement rates and paleoearthquakes in an active rift. Geology 34 (10), 865–868.
Nicol, A., Walsh, J., Mouslopoulou, V., Villamor, P., 2009. Earthquake histories and Holocene acceleration of fault displacement rates. Geology 37, 911–914.
Nogrady, B., 2017. As Global Demand for Electricity Grows, Geothermal Energy Heats up. accessed 4 February 2019. https://ensia.com/features/geothermal-energy/.
Pearce, N.J., Abbott, P.M., Martin-Jones, C., 2014. Microbeam methods for the analysis of glass in fine-grained tephra deposits: a SMART perspective on current and future trends. Geol. Soc. Spec. Publ. 398, 29–46. https://doi.org/10.1144/SP398.1.
Pillans, B.J., McGlone, M.S., Palmer, A.S., Mildenhall, D.C., Alloway, B.V., Berger, G.W., 1993. The Last Glacial Maximum in central and southern North Island, New Zealand: a palaeoenvironmental reconstruction using the Kawakawa Tephra Formation as a chronostratigraphic marker. Palaeogeogr. Palaeoclimatol. Palaeoecol. 101, 283–304.
Preston, L.J., Benedix, G.K., Genge, M.J., Sephton, M.A., 2008. A multidisciplinary study of silica sinter deposits with applications to silica identification and detection of fossil life on Mars. Icarus 198, 331–350. https://doi.org/10.1016/j.icarus.2008.08.006.
Reyners, M., Eberhart-Phillips, D., Stuart, G., 2007. The role of fluids in lower-crustal earthquakes near continental rifts. Nature 446 (7139), 1075.
Rimstidt, J.D., Cole, D.R., 1983. Geothermal mineralization. I, the mechanism of formation of the Beowawe, Nevada, siliceous sinter deposit. Am. J. Sci. 283, 861–875.
Rowland, J.V., Sibson, R.H., 2004. Structural controls on hydrothermal flow in a segmented rift system, Taupo Volcanic Zone, New Zealand. Geofluids 4, 259–283.
Sase, T., Hosono, M., Utsugawa, T., Aoki, K., 1988. Opal phytolith analysis of present and buried volcanic ash soils at Te Ngae Road tephra section, Rotorua Basin, North Island, New Zealand. Quat. Res. 27, 153–163.
Selby, M.J., 1967a. Erosion by high intensity rainfalls in the lower Waikato. Earth Sci. J. 1 (2), 153–156.
Selby, M.J., 1967b. Aspects of the geomorphology of the greywacke ranges bordering the lower and middle Waikato basins. Earth Sci. J. 1 (1), 37–56.
Shane, P.A.R., Smith, V.C., Nairn, I.A., 2005. High temperature rhyodacites of the 36 ka Hauparu pyroclastic eruption, Okataina Volcanic Centre, New Zealand: change in a silicic magmatic system following caldera collapse. J. Volcanol. Geoth. Res. 147, 357–376.
Shane, P.A.R., Nairn, I.A., Martin, S.B., Smith, V.C., 2008. Compositional heterogeneity in tephra deposits resulting from the eruption of multiple magma bodies: implications for tephrochronology. Quat. Int. 178, 44–53.
Simmons, S.F., Keywood, M., Scott, B.J., Keam, R.F., 1993. Irreversible change of the Rotomahana-Waimangu hydrothermal system (New Zealand) as a consequence of a volcanic eruption. Geology 21, 643–646.
Smith, V.C., Shane, P.A.R., 2002. Geochemical characteristics of the widespread Tahuna tephra. N. Z. J. Geol. Geophys. 45, 103–107. https://doi.org/10.1080/00288306.2002.9514962.
Smith, V.C., Shane, P.A.R., Nairn, I.A., 2004. Reactivation of a rhyolitic magma body by new rhyolitic intrusion before the 15.8 ka Rotorua eruptive episode: implications for magma storage in the Okataina Volcanic Centre, New Zealand. J. Geolog. Soc. London 161, 757–772.
Smith, V.C., Shane, P., Nairn, I.A., 2005. Trends in rhyolite geochemistry, mineralogy, and magma storage during the last 50 kyr at Okataina and Taupo volcanic centres, Taupo Volcanic Zone, New Zealand. J. Volcanol. Geoth. Res. 148, 372–406.
Stirling, M., McVerry, G., Gerstenberger, M., Litchfield, N., Van Dissen, R., Berryman, K., Barnes, P., Wallace, L., Villamor, P., Langridge, R., Lamarche, G., Nodder, S., Reyners, M., Bradley, B., Rhoades, D., Smith, W., Nicol, A., Pettinga, J., Clark, K., Jacobs, K., 2012. National Seismic Hazard Model for New Zealand: 2010 update. Bulletin of the Seismological Society of America 102, 1514–1542.
Vandergoes, M.J., Hogg, A.G., Lowe, D.J., Newnham, R.M., Denton, G.H., Southon, J., Barrell, D.J.A., Wilson, C.J.N., McGlone, M.S., Allan, A.S.R., Almond, P.C., Petchey, F., Dalbell, K., Dieffenbacher-Krall, A.C., Blaauw, M., 2013. A revised age for the Kawakawa/Oruanui tephra, a key marker for the Last Glacial Maximum in New Zealand. Quat. Sci. Rev. 74, 195–201.
Villamor, P., Berryman, K., 2001. A late Quaternary extension rate in the Taupo Volcanic Zone, New Zealand, derived from fault slip data. N. Z. J. Geol. Geophys. 44, 243–269. https://doi.org/10.1080/00288306.2001.9514937.
Villamor, P., Berryman, K.R., 2006. Evolution of the southern termination of the Taupo Rift, New Zealand. N. Z. J. Geol. Geophys. 49, 23–37. https://doi.org/10.1080/00288306.2006.9515145.
Villamor, P., Ries, W., Zajac, A., 2010. Rotorua District Council hazard studies: active fault hazards. In: GNS Science Consultancy Report 2010/182, pp. 28.
Villamor, P., Berryman, K.R., Nairn, I.A., Wilson, K., Litchfield, N., Ries, W., 2011. Associations between volcanic eruptions from Okataina volcanic center and surface rupture of nearby active faults, Taupo rift, New Zealand: insights into the nature of volcano-tectonic interactions. Geol. Soc. Am. Bull. 123, 1383–1405. https://doi.org/10.1130/B30184.1.
Villamor, P., Berryman, K.R., Ellis, S.M., Schreurs, G., Wallace, L.M., Leonard, G.S., Langridge, R.M., Ries, W.F., 2017. Rapid evolution of subduction-related continental intraarc rifts: the Taupo Rift, New Zealand. Tectonics 36 (10), 2250–2272.
Vucetich, C.G., Pullar, W.A., 1969. Stratigraphy and chronology of Late Pleistocene volcanic ash beds in central North Island, New Zealand. N. Z. J. Geol. Geophys. 12, 784–837.
Wallace, L.M., Beavan, J., McCaffrey, R., Darby, D., 2004. Subduction zone coupling and tectonic block rotations in the North Island, New Zealand. J. Geophys. Res. 109, B12406. https://doi.org/10.1029/2004JB003241.
Wilson, C.J.N., 1985. The Taupo eruption, New Zealand II. The Taupo ignimbrite. Philos. T Roy. Soc. A 314, 229–310. https://doi.org/10.1098/rsta.1985.0020.
Wilson, C.J.N., 1993. Stratigraphy, chronology, styles and dynamics of late Quaternary eruptions from Taupo volcano, New Zealand. Philos. T Roy. Soc. A 343, 205–306. https://doi.org/10.1098/rsta.1993.0050.
Wilson, C.J.N., Walker, G.P., 1985. The Taupo eruption, New Zealand I. General aspects. Philos. T Roy. Soc. A 314, 199–228. https://doi.org/10.1098/rsta.1985.0019.
Wilson, C.J.N., Houghton, B.F., McWilliams, M.O., Lanphere, M.A., Weaver, S.D., Briggs, R.M., 1995. Volcanic and structural evolution of Taupo Volcanic Zone, New Zealand: a review. J. Volcanol. Geoth. Res. 68, 1–28.
Wilson, C.J.N., Rhoades, D.A., Lanphere, M.A., Clavert, A.T., Houghton, B.F., Weaver, S.D., Cole, J.W., 2007. A multiple-approach radiometric age estimate for the Rotoiti and Earthquake Flat eruptions, New Zealand, with implications for the MIS 4/3 boundary. Quat. Sci. Rev. 26, 1861–1870/.
Wilson, C.J.N., Gravley, D.M., Leonard, G.S., Rowland, J.V., 2009. Volcanism in the central Taupo Volcanic Zone, New Zealand: tempo, styles and controls. In: Thordarson, T., Self, S., Larsen, G., Rowland, S.K., Hoskuldsson, A. (Eds.), Studies in Volcanology: the Legacy of George Walker. Special Publications of IAVCEI. 2. Geological Society, London, pp. 225–247.